Investigating the role of *FOSL1*/FRA1 in *BRAF*-V600E patient-derived colorectal cancer organoids

Report

Minor Research Project
MSc Regenerative Medicine & Technology

Polina Deenichina

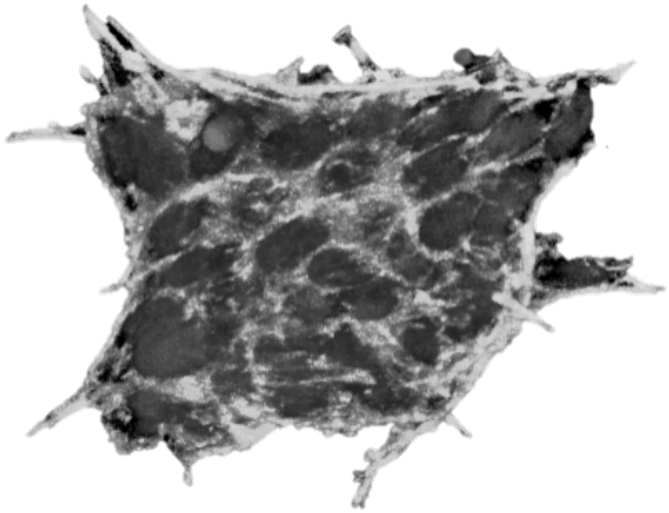

Colorectal cancer organoid

`

Laboratory Translational Oncology of University Medical Centre Utrecht

Daily supervision:
Layla El Bouazzaoui

First Examiner:
Prof. Onno Kranenburg

Second Examiner:
Dr. Jeanine Roodhart

UMC Utrecht

Utrecht University

Table of Contents

Summary

Cells are the building blocks of all life and different types of cells combine to make up tissues and organs. Epithelial cells line the inside of the large intestine that includes the colon and the rectum. Each cell is programmed by a genetic code that gives instructions on every decision that the cell has to make, including division, growth, movement and death. These cellular processes are accomplished by genes that are being expressed according to the genetic code. When genes are expressed, proteins are produced that make up different parts of cells. The cells divide to give rise to new cells with the same characteristics as the mother cell. If there is a mistake in the genetic code also called a mutation, the cells could divide uncontrollably resulting in a massive formation referred to as a tumour. If the cells within the tumour accumulate more mutations, this could lead to some cells detaching and migrating to a different tissue in the body to form more tumours called metastases. Forming tumours and developing metastasis are part of the cancer disease, and cancer with metastases is called metastatic. The originating tissue of cancer gives it its name. When the cancer develops from the epithelium of the colon or rectum, it is referred to as colorectal cancer (CRC). CRC can be classified by specific mutations that often co-occur together. An aggressive and deadly type of metastatic CRC is highly associated with a mutation in the *BRAF* gene, that is abbreviated V600E, that forms a mutant BRAF protein. The V600E mutation is correlated with other genes, namely *FOSL1*. *FOSL1* is known to be dysregulated in metastatic cancers, but the mechanism is poorly understood. The aim of this report is to understand how *FOSL1* and its gene product called FRA1 are involved in metastatic CRC that has the V600E mutation in the *BRAF* gene. To address this aim we used small 3D spherical models of cancer that are referred to as organoids. The organoids were generated from patient-derived colorectal tumours positive for the *BRAF*-V600E mutation. The *BRAF*-V600E cancerous organoids were used in this study along with organoids that were corrected for the V600E mutation and produced a normal BRAF protein. We used anti-cancer drugs called chemotherapy to block the mutated BRAF protein and identified that FRA1 was also blocked. We mimicked the metastatic process and found out that the *BRAF*-V600E mutation causes the spherical organoids to change shape and to form sprouts protruding from the spheres. The shape of cells and organoids is called morphology. The sprouting morphology was reversed to spherical or normal when BRAF was blocked with chemotherapy. From that we concluded that the V600E mutation causes the change in shape possibly in combination with FRA1. We performed further experiments to understand how FRA1 interacts with other genes involved in metastasis, but we did not find a connection.

Abstract

In colorectal cancer (CRC) progression, the *BRAF*-V600E activating mutation is characteristic of the serrated pathway. In combination with other genomic instabilities, *BRAF*-V600E could be a poor prognostic marker associated with low survival in metastatic CRC. The *FOSL1* gene was identified to be preferentially upregulated in CRC patient-derived organoids carrying the *BRAF*-V600E mutation compared to *BRAF* wild type organoids, making it a potential effector of the mutation. *FOSL1* and its gene product named FRA1 are present in tumour tissues in different types of cancers, but not in healthy epithelium. FRA1 is expressed on the invasive front of tumours and in metastatic lesions, and its expression is positively correlated with the number of metastases. *FOSL1* was found to be dispensable for survival but was required for the metastatic spread of epithelial cells *in vivo*. The proposed mechanisms by which *FOSL1* is involved in metastasis are via epithelial to mesenchymal transition (EMT) and cell motility. On molecular level, FRA1 is known to coimmunoprecipitate with the *EZH2* promoter, that is a major driver of (EMT) and stemness, and a core component of the PRC2 complex, along with SUZ12 and EED. Although there is strong evidence that implicates FRA1 in metastasis, the molecular mechanisms are still elusive. In this paper, we sought to elucidate the role of FRA1 in relation to the *BRAF*-V600E mutation to identify the pathological mechanisms associated with metastatic CRC by employing a model system of patient-derived CRC organoids mutant for the *BRAF*-V600E. Immunoblotting revealed that FRA1 expression and organoid morphology in a metastatic-mimicking environment containing Collagen I, are BRAF-dependent. Inhibition of *FOSL1* transcription with small interfering RNA did not have an effect on PRC2 core component gene transcription and protein expression. Protein-DNA interactions between FRA1 and *EED*, *EZH2* and *SUZ12* could not be identified via chromatin immunoprecipitation and RT-PCR.

Key words: colorectal cancer • metastasis • FRA1 • *BRAF*-V600E • organoid sprouting

Abbreviations

AP-1 = Activating protein 1
APC = Adenomatous polyposis coli
BRAF = Murine sarcoma viral oncogene homolog B
CMYC = Cellular myelocytomatosis oncogene
CRC = Colorectal cancer
EED = Embryonic ectoderm development
EGFR = Epidermal growth factor receptor
ERK = Extracellular signal-regulated kinase
EZH2 = Enhancer of zeste 2 polycomb repressive complex 2 subuint
FOSL1 = FOS-like 1
FRA1 = FOS-related antigen 1
GAPDH = Gyceraldehyde-3-phosphate dehydrogenase
H3 = Histone 3
H3K27me3 = Histone 3 trimethylated at lysine 27
KRAS = Kirsten rat sarcoma virus
MAPK = Mitogen-activated protein kinase
MEK = Mitogen-activated protein kinase 1
p. cMYC = phosphorylated cMYC
p. ERK = phosphorylated ERK
p. FRA1 = phosphorylated FRA1
PRC2 = Polycomb repressive complex 2
RNF43 = Ring finger protein 43
ROCK = Rho-associated coiled-coil containing protein kinase
RSK = Ribosomal s6 kinase
SUZ12 = Polycomb repressive complex 2 subunit
TP53 = Tumour protein p53
Wnt = Wingless-related integration site

Introduction

Colorectal cancer

Colorectal cancer (CRC) is among the world's deadliest cancers [1–3], with a higher degree of incidences in developed countries [4,5]. Due to its physiological origins in the large intestine that includes the colon and the rectum, sporadic CRC is often regarded a function of the western lifestyle encompassing unhealthy dietary habits, chronic stress, antibiotic-induced alterations to the gut microbiota, next to other CRC risk factors such as family history and longstanding bowel inflammation [6,7]. The majority of CRC cases are assumed to arise from cancer stem cells (CSCs) or stem-cell-like cells residing at the base of the colonic crypts [8]. Accumulation of genetic and epigenetic alterations within the CSCs drive various histological changes including hyperproliferation leading to the formation of a neoplastic precursor lesion or a benign polyp [9]. If undetected, the polyp cells can acquire malignant mutations and progress into metastatic CRC [7–9]. According to the National Cancer Institute, the survival of CRC patients baring distant metastasis is less than 20% beyond 5 years from diagnosis in the US [10]. CRC, like other solid tumours, is a heterogeneous disease in which different subtypes are underlyied by specific molecular and/or clinical features. CRC progression is determined by two major precursor lesion pathways characterised by different types of genomic instabilities 1) the traditional adenoma-carcinoma pathway and the 2) 'alternative' serrated neoplasia pathway (Fig. 1).

The conventional adenoma-carcinoma sequence

The conventional adenoma-carcinoma sequence is well-understood and approximately 90% of CRCs arise from it [11]. The model was postulated by Fearon and Vogelstein as a stepwise pattern of activation and inactivation of key oncogenes and tumour suppressors, respectively (Fig. 1) [12]. A key event for adenoma initiation is thought to be the inactivation of the tumour suppressor gene *APC* that leads to the activation of the Wnt/b-catenin pathway [12–17]. APC is a key member of the b-catenin destruction complex involved in the suppression of Wnt/b-catenin signalling [18]. When mutated or transcriptionally silenced, the destruction complex is no longer active and b-catenin is stabilised thereby accumulating in the cytoplasm [13,14]. Once saturated in the cytoplasm, b-catenin translocates to the nucleus where it interacts with canonical Wnt targets to promote 'stemness' characterised by proliferation, migration, invasion, and metastasis, which result in the unrestrained proliferation of the adenomatous polyp [19–21]. Following *APC* loss, a turning point in the adenoma-carcinoma sequence, is acquiring an activating mutation in *KRAS* which is a member of the MAPK pathway. KRAS is a small GTPase of the RAS family of proto-oncoproteins and acts as a relay for signals originating at receptor tyrosine kinases such as the EGFR family [12,22,23]. Upon binding of mitogens, EGFR is activated initiating a phosphorylation chain reaction through RAS, RAF, MEK and finally ERK. Phosphorylated ERK can translocate to the nucleus and interact with many transcription factors to initiate transcriptional programs regulating proliferation, differentiation, and apoptosis [24]. Oncogenic KRAS promotes constitutive signalling of the MAPK pathway without the presence of growth factors, synergising with aberrant Wnt/b-catenin signalling, to drive transformation from adenoma to carcinoma [25,26]. Both pathways are highly conserved and regulate essential cell properties including stem cell maintenance, growth, and proliferation. The co-activation of Wnt/b-catenin and

MAPK, is a prerequisite for accumulating further mutations in other key genes including the tumour suppressor *TP53*, to drive malignant progression [12,27]. Although the original model presents mutation events in a temporal manner, there is a consensus that not the chronological order of mutations, but their accumulation and synergistic effect is more important for developing CRC.

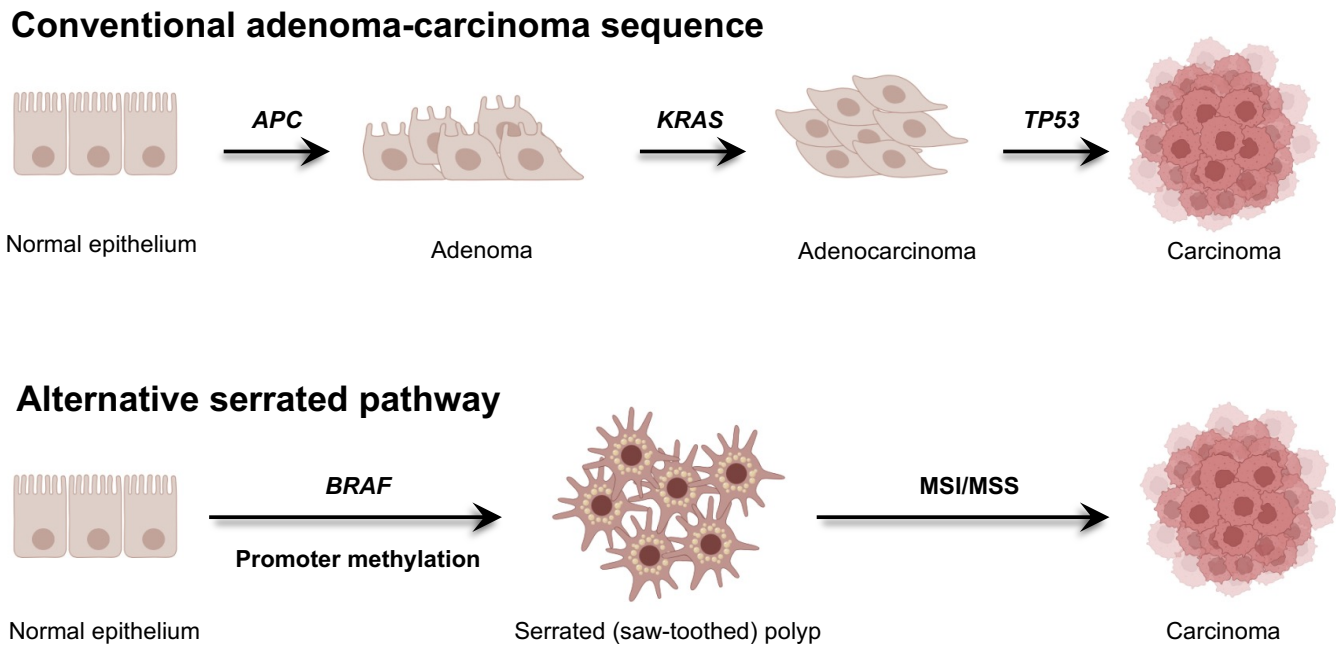

Figure 1. Major molecular pathways in colorectal cancer.

The conventional adenoma-carcinoma sequence is described as a stepwise accumulation of genome alterations in key tumour suppressor genes and oncogenes that lead to the oncogenic transformation from normal epithelium to malignancy. The alternative serrated pathway is characterised with its distinct serrated morphology, and mutations within the MAPK pathway, specifically in the *BRAF* gene, combined with silencing of tumour suppressor genes via promoter methylation.

The alternative serrated neoplasia pathway

Serrated tumours were first described by Jass and Smith in 1992, but only in the past decade the serrated pathway has been recognised as another significant route leading to CRC, and therefore the molecular underworks are still elusive [28,29]. Although only ~15% of all sporadic CRC arise via the serrated pathway, it predicts a more aggressive phenotype and an overall worse prognosis compared to conventional adenocarcinomas, particularly in late-stage disease [30]. The serrated pathway is characterised by development of a serrated precursor lesion often associated with promoter methylation of key tumour suppressor genes and microsatellite stability status, whereby microsatelite instable cancers (MSI) are associated with a better prognosis compared to microsatellite stable (MSS) cancers [31,32].

Whereas alterations in *APC* and *KRAS* are common for the adenoma-carcinoma sequence, in the serrated pathway this is rarely the case [33–35]. Mutations in the *BRAF* gene occur early in tumorigenesis and are highly associated with the serrated neoplasia pathway [36]. BRAF is a serine-threonine kinase that is directly downstream of KRAS and represents the top-level element of the MAPK cascade [37]. Oncogenic mutations in either *KRAS* or *BRAF* result in the constitutive activation of the MAPK pathway. Therefore, mutations in either rarely occur together in the same colorectal cancer and are considered mutually exclusive [38–40]. This is likely because there is no selective advantage for a cell to develop a second mutation in the same pathway when the first is already present due to redundancy. Rather, co-activation of two different pathways such as Wnt/b-catenin and MAPK is more advantageous evident by their frequent co-occurance in CRC [41–43]. Of note, there is a trend of specific mutations to combine. For example, *APC* and *KRAS* in the adenoma-carcinoma sequence, *BRAF* and *RNF43* in the serrated pathway [42,44]. *RNF43* is a negative regulator of the Wnt/b-catenin pathway, and inactivating mutations within *RNF43* lead to upregulation of Wnt signalling [45,46]. Although both MAPK and Wnt/b-catenin cascades are affected by either combination of mutations, it has been shown that

BRAF and *RNF43* are negative prognostic factors in metastatic CRC [43,47].

The BRAF-V600E mutation

The most common mutation (~95%) within the *BRAF* gene in CRC is a single nucleotide substitution that leads to an amino acid change from valine to glutamic acid (V600E) and is associated with poor survival prognosis in the metastatic stage compared to BRAF wildtype cancers [30–32,47,48]. This occurs within the activating domain of BRAF increasing its kinase activity 10 times compared to wildtype, and thereby constitutively activating the MAPK pathway, independent of presence of mitogens [22,48]. Although oncogenic mutations in *KRAS* also lead to overactivation of the MAPK pathway, it has been shown that *BRAF* carrying V600E conferred more elevated levels of phosphorylated MEK and phosphorylated ERK, compared to mutant KRAS, highlighting the potency of V600E in upregulating the MAPK pathway [47,49].

Looking into direct ERK targets that are differentially expressed in *BRAF* vs *KRAS* mutants in CRC, the Kranenburg group identified *FOSL1* as an interesting target. *FOSL1* was upregulated in *BRAF*-mutant CRC organoids in a dataset of *BRAF*-mutant vs *KRAS*-mutant organoids (Sup. Fig. 1, A). Additionally, in a cohort of CRC patient biopsies upregulation of *FOSL1* was also observed in *BRAF*-mutant CRCs compared to *BRAF*-wildtype (*BRAF*-wt) CRCs (Sup. Fig. 1, B), also in agreement with results from the large TCGA publicly available dataset (Sup. Fig. 1, C). These data suggest that *FOSL1* is a *BRAF*-V600E specific effector.

FOSL1/FRA1

FOSL1 codes for a protein called FRA1 which is a member of the FOS family of proteins [50]. The FOS proteins form heterodimers with other proteins (e.g., the JUN family) to become a functioning component of the AP-1 transcription factor complex (Fig. 2, A) [51–53]. AP-1 is heterogenous because there are numerous protein-protein combinations, and it has been challenging to assign a specific well-defined biological function, however, it has been shown that is involved in cell cycle progression, apoptosis and transformation, among others [50,51]. The differential combination of the different AP-1 components (Fig. 2, B) allows tissue-specific and temporal regulation of gene expression, and for this reason, family members of the transcription factor complex are considered to be proto-oncogenes [54]. AP-1 is regulated by multiple pathways, but it has been shown that MAPK signalling is involved in the transcriptional and post-translational modification of specific AP-1 components, such as FRA1 [55,56].

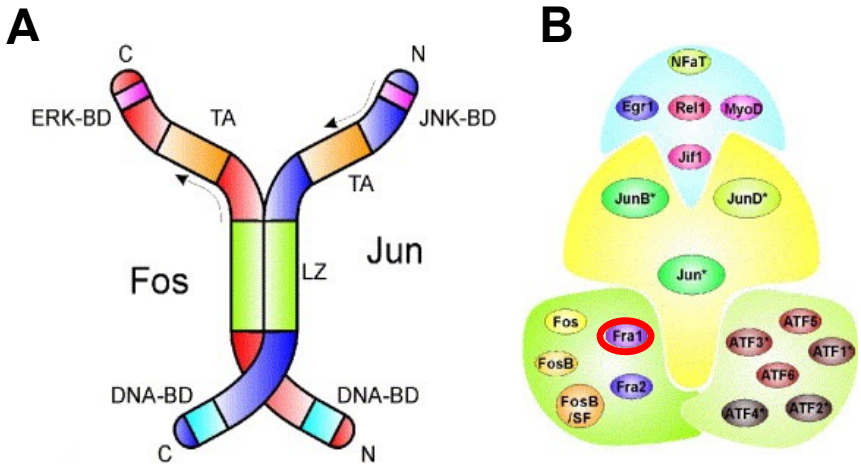

Figure 2. AP-1 transcription factor dimers.

(A) The classical c-JUN/c-FOS heterodimer, containing the DNA binding domains (DNA-BD), the leucine zipper (LZ) region, the transcription-activating or transactivating module (TA), and the binding domains for the mitogen-activated protein kinases, ERK (ERK-BD) in the case of c-Fos, and JNK (JNK-BD) for c-Jun.

(B) A summary of dimer-forming interactions between different groups of AP-1 transcription factor families. Members of the c-Jun family can form various heterodimers with the adjacent c-Fos family (left), the ATF family (right) or a large group of transcription factors including Egr1, Rel1, Zif1, MyoD or NFAT. All Jun family members and most ATF family members, marked with *, are also known to form homodimers. The ATF transcription factors also form heterodimers with the Fos family. The figure and legend were adapted from Raivich & Behrens, 2006.

Although FRA1 participates in several signalling cascades, only three kinases, namely ERK2, RSK2 and ERK5 (effectors of MAPK) interact with FRA1 directly. ERK2 phosphorylates Serine on positions 252 and 265, RSK also phosphorylates Serine 265 and ERK5 phosphorylates Threonine 230 in human FRA1 [58–62]. In all three cases, phosphorylation favours the stabilisation of FRA1 and prevents it from proteasomal degradation [63]. It is also known that threonine phosphorylation enhances FRA1 biological activity, and mutating threonine residues inhibits the transcriptional activity of FRA1 [58,59].

Although FRA1 is downstream of KRAS and BRAF, the Kranenburg group previously demonstrated that *FOSL1* is preferentially upregulated in *BRAF*-V600E mutants (Sup. Fig. 1, B, C). In addition, the same group used a CRC patient-derived organoid (PDO) line (T10) that carries a *BRAF*-V600E mutant allele to study the effects of the V600E mutation in CRC. In this PDO, they used CRISPR technology to correct the *BRAF*-mutant V600E allele to wildtype (BC1, BC2). A non-corrected BRAF clone of T10 (NC) that underwent the CRISPR process was included as an additional control. Comparing *BRAF*-V600E mutant and the CRISPR-engineered *BRAF*-corrected CRC organoids revealed that *FOSL1* and its target genes were highly upregulated in *BRAF*-V600E clones (Sup. Fig. 2, A-C). On protein level, the *BRAF*-corrected clones had low basal expression of phosphorylated ERK and FRA1 and compared to *BRAF*-V600E mutants (Sup. Fig. 2, D). Furthermore, the specific inhibition of BRAF with either vemurafenib or encorafenib abolished phosphorylated ERK and FRA1 expression in *BRAF*-mutant CRC organoids (Sup. Fig. 2, D). Treatment with encorafenib ceased FRA1 expression and activation (phosphorylation) in T10 in a time-dependent manner (Sup. Fig. 2, E). These results confirmed previous findings that FRA1 is directly regulated by post-translational phosphorylation by ERK of the MAPK cascade, and that FRA1 is specifically overexpressed due to the V600E activation mutation in the *BRAF* gene. Being heavily implicated in the *BRAF*-V600E signalling, FRA1 is a potential candidate for the aggressive phenotype observed in metastatic *BRAF*-V600E-positive cancers.

FOSL1/FRA1 in cancer

FOSL1 overexpression is characteristic for the most aggressive forms of cancer such as triple-negative breast cancer and malignant glioma among others [64–68]. FRA1 expression is also highly correlated with the number of metastasis in the liver and lymph nodes [69,70]. Moreover, immunohistochemistry revealed that FRA1 was not detected in healthy epithelial cells, but was present in lesions, whereby the strongest FRA1 expression was in marginal invasive cancer cells, and FRA1 expression was higher in liver metastases than in primary tumours [70–73]. Although FRA1 expression in tumours is higher than in healthy tissue, it has been shown that it is not essential for tumorigenic growth and proliferation in CRC [74]. However, there is strong evidence that implicates FRA1 in the invasive and metastatic ability of CRC. FRA1 was found to be responsible for the motility and invasive properties of colon carcinoma cells *in vitro* in an ERK-MAPK-dependent manner (Vial et al., 2003). Iskit et al., demonstrated convincing evidence that FRA1 is a key driver of colon cancer metastasis *in vivo*, whereby mice injected with FRA1-depleted epithelial Caco-2 cells had a significantly reduced metastatic burden compared to controls and FRA1 was crucial for the expansion of established metastatic lesions [74]. These findings suggest that FRA1 is heavily involved in the metastatic cascade in different types of cancer.

To tackle the molecular involvement of FRA1 in metastasis, gene ontology analysis revealed that *FOSL1* overexpression and silencing affect gene programmes in two major categories, namely, epithelial to mesenchymal transition (EMT) and cell adhesion [70,76–78]. EMT and evading anchorage-dependent systems are hallmarks of metastatic progression [79]. In developing tumours, EMT coincides with budding whereby tumour cells detach from the invasive front of the tumour and invade the basement membrane [80]. Then cells enter the bloodstream and are disseminated across the body. Cancer cells entering the circulation is a prerequisite for metastases development [81]. In order to colonise, cells undergo mesenchymal to epithelial transition (MET) and invade the tissues [82]. Being epithelial in origin, CRC cells losing epithelial markers to gain mesenchymal, is thought to be an early step in the metastatic cascade. Of note, overexpression of *FOSL1* in epithelial cells was shown to cause changes in cell morphology characteristic of EMT. On one hand overexpression of *FOSL1* led to the suppression of epithelial biomarkers (e.g., E-cadherin), integrins and cell junction proteins. In turn, their downregulation impaired cell polarity and paracellular transport in CRC cells [70]. On the other hand, endothelial markers (e.g., Vimentin) and matrix-degrading enzymes (e.g., metalloproteinases) were induced. As a result, the *FOSL1*-overexpressing cells formed numerous protrusions and migrated. When transplanted in mice, these cells efficiently colonised the lung and transformed into vascularised tumours [77]. The opposite effect was observed when *FOSL1* was silenced. Epithelial features were upregulated whereby cells flattened out and suspended their invasive behaviour, lost tumorigenicity and restored tight junctions [70,77,78,83].

Although FRA1 seems to be deregulated in EMT and cell polarity, the molecular mechanisms are still elusive. There is evidence that links FRA1 to EMT and stemness-like phenotypes via *EZH2*. EZH2 is an

epigenetic driver of EMT, and its overexpression is correlated to colonic metastasis in an ERK-dependent manner, similar to FRA1 [75,84]. EZH2 is essential for the enzyme function of the Polycomb repressive compex 2 (PRC2) along with the other core components EED and SUZ12 [85]. PRC2 epigenetically represses promoters through thrimethylation of histone H3 at Lysine 27 residue (H3K27me3) to regulate cellular identity, stem-cell plasticity and proliferation [86]. *EZH2* was found to bare binding sites for FRA1 in its promoter region, and chromatin immunoprecipitation confirmed that FRA1 and C-JUN were occupying the *EZH2* promoter *in vitro* [84]. These findings suggest a potential FRA1-mediated regulation of the PRC2 complex through *EZH2* that could contribute to epithelial transformations in malignant cancer. Overall, there is a growing body of evidence reviewed by Jiang et al., 2019 and Sobolev et al., 2022 that implicate *FOSL1*/FRA1 as a major player in metastasis in various cancers primarily through increased cell motility that is determined by different mechanisms where FRA1 might be involved.

BRAF-V600E is associated with an aggressive phenotype in metastatic CRC. FRA1 is specifically upregulated by the *BRAF*-V600E signalling and is involved in metastasis potentially contributing to this phenotype. In this research we aim to unravel the effects of *BRAF*-V600E-mediated overactivation of FRA1 on cell morphology and interaction with the PRC2 core component genes. To address these aims we must verify that 1) FRA1 is a direct target of MAPK pathway, and more specifically, that FRA1 is induced by *BRAF*-V600E signalling; 2) *BRAF*-V600E-induced FRA1 contributes to metastatic characteristics; 3) FRA1 is contributing to an aggressive stem cell-like state via activation of the PRC2 complex. To answer these questions, we used the previously established *BRAF*-V600E mutant (T10, NC) and BRAF-corrected (BC1, BC2) organoid lines as model systems for the *BRAF*-V600E mutant subtype of CRC and incorporated specific BRAF and *FOSL1* inhibitors. We confirmed that FRA1 is a direct target of *BRAF*-V600E signalling through ERK-mediated phosphorylation of FRA1. To understand how FRA1 is involved in metastasis, we developed an invasion-promoting assay using Collagen I, as it is known to be an integral component in the metastatic extracellular microenvironment [89–91]. The Collagen I-rich 3D assays revealed that CRC organoids positive for the BRAF-V600E mutation presented with a morphology associated with invasion, and *BRAF*-wildtype (*BRAF*-wt) did not. Upon pharmacological inhibition of BRAF, the invasive phenotype was partially abolished, confirming that *BRAF*-V600E is promoting cellular aberrations possibly through FRA1. The molecular involvement of FRA1 with the PRC2 genes was assessed via a protein-DNA interaction assay (ChIP), followed by a real time polymerase chain reaction (RT-PCR) analysis. Due to technical difficulties with the ChIP and the RT-PCR, we were unable to answer if FRA1 occupies the PRC2 promoters in a BRAF-dependent manner. Although the ChIP-RT-PCR was inconclusive, we did not find any relation of FRA1 and the PRC2 components on a protein or *mRNA* level, suggesting an alternative mechanism by which FRA1 is involved in metastatic CRC. CMYC is a known target of the MAPK pathway and is also a known regulator of the PRC2 complex in a BRAF-dependent manner [92]. Due to the overlap with FRA1, cMYC was used as a positive control in all experiments.

Our research is in line with previous findings that expression of FRA1 is BRAF-dependent, and that the V600E mutation is associated with an invasive cell morphology in Collagen I, possibly through FRA1. We did not find a link between FRA1 and PRC2, however, that narrows the targets within the FRA1 interactome that might be involved in CRC progression.

Materials & Methods

Information about materials and primer sequences can be found in Supplementary Tables 1 and 2, respectively.

Organoid lines and culture procedures

Organoid lines

The *BRAF*-V600E mutant organoid line referred to as T10 (original name: HUB-02-B2-040) and the healthy colon-tissue-derived H040-N were generated from colorectal cancer and colorectal healthy biopsies, respectively, from the same patient. The T10 line was used to generate organoid clones with a restored *BRAF* wildtype allele (*BRAF*-wt) with CRISPR/ LbCpfl via homology-directed repair. Additionally, another clone of T10 referred to as NC non-corrected, also underwent the CRISPR process without being corrected for the V600E mutation, and therefore was used as an additional control.

BRAF-V600E Genotyping

To check whether the lines were stably corrected or non-corrected, they were genotyped for the *BRAF* region (Sup. Table 2; 12). DNA was isolated from T10, NC, BC1 and BC2 organoid lines using the QIAamp DNA Micro Kit. After measuring DNA concentration

on a Nanodrop 2000, a PCR was run to amplify the regions of interest following the GoTaq DNA Polymerase protocol.

Single 25 μl reaction		Run protocol	
5x Green GoTaq Buffer	5 µL	94ºC	5’
$MgCl_2$	1.75 µL	55ºC	1’
dNTPs (10 mM)	0.75 µL	72ºC	1’30’’
10 µM Forward primer	1 µL	Go To Step 2 27x	
10 µM Reverse primer	1 µL	94ºC	30’’
GoTaq Polymerase	0.125 µL	58ºC	40’’
Genomic DNA template	1 µL	72ºC	50’’
Nucelase-free water	14.375 µL	72ºC	10’
		4ºC	∞

Then the PCR products were separated via electrophoresis on a 1 % agarose gel. Bands with the correct size were cut out from the gel and DNA was purified using Roche’s High Pure PCR Product Purification Kit. The purified DNA was sent for Sanger sequencing in reactions of 2.5 µL with a primer targeting a sequence within the PCR product and 7.5 µL DNA. Then the results were aligned in Benchling where sequenced transcripts were compared to the correction template.

Organoid culture

Organoids were cultured in 70% basement membrane extract (BME) and 30% Advanced DMEM/F12 supplemented with 1% Penicilin/Streptomycin, 1 M Hepes and 1% Glutamax (referred to as Basal Media or BM). Additionally, 1x B27, 10% Noggin-conditioned medium, 1.25 mM N-acetylcysteine, 10 mM Nicotinamide, 0.5 µM A8301, 10 µM SB202190 and 50 mg/mL EGF were added to the BM media (referred to as Enriched Medium or EM). EM was used to refresh organoids every 2-3 days. Depending on the seeding ratio and growth speed, organoids were passed approximately every 7 days in ratios between 1:3 and 1:6. To be passaged, droplets containing the organoids were mechanically disrupted and collected in cold BM media. They were centrifuged at 1800 RPM and the media was aspirated. Then organoids were either mechanically disrupted with a P10 tip inside a P1000 tip, or with the use of TrypLE enzyme for single cell dissociation. Organoids were incubated with prewarmed 1 mL of Tryple E at 37ºC between 5 and 10’. The enzyme reaction was deactivated with 10 mL cold BM. After repelleting and supernatant aspiration, organoids were mixed with BM:BME (30:70) and seeded in ~5 µL hanging droplets in 6-well plates at 37ºC for 1 h. Upon single cell dissociation, EM media supplied with 10 μM ROCK inhibitor Y-27632. For the non-mutant healthy H040-N line, the EM was supplied additionally with 20% R-spondin 1-conditioned medium and 1% Wnt surrogate conditioned medium.

BRAF inhibition

Prior to adding BRAF inhibitors organoids were growth-factor-starved in a low serum media overnight. Then, encorafenib or vemurafenib were added to a final concentration of 1 µM to *BRAF*-mutant lines (T10, NC) and DMSO was added for control treatment to *BRAF*-corrected lines (BC1, BC2).

Small interference RNA

Small interference RNA (siRNA) was prepared prior to experiment according to manufacturer’s instructions. SiRNA concentration was verified using UV spectrophotometry at 260 nm: siControl = 233 ng/µL, siFOSL1 = 300 ng/µL.

Sample preparation

For this experiment 2 wells of ~$1.5x10^6$ of each T10 and NC were seeded in 6-well plates as per standard culturing regiment described above. After growing at almost full capacity of the BME droplets, the organoids were dissociated into single cells with TrypLE and moved to ultra-low adherent plates in 1 mL suspensions. The cells were transfected according to Interferin transfection reagent protocol for suspension cells. For 1 mL of cell suspension, 200 µL of Opti-MEM were mixed with 12 µL of Interferin and siRNA Control

(siCntrl) or siRNA against *FOSL1* (siFOSL1) at a final concentration on 1.5 µM. The cells were incubated at 37ºC for 6 hours and they were resuspended hourly to ensure homogenous transfection. At the end of the treatment, the cells were collected and seeded into BM:BME matrix as per standard procedure.

RNA isolation

24 hours after siRNA treatment, cells were collected in 15 mL falcon tubes and resuspended with a 23-gauge needle (0.6 mm x 30 mm) under pressure and lysed with cell lysis buffer (RLT + b-mercaptoethanol). The rest of the RNA isolation procedure was carried out following the RNeasy Micro Kit's protocol. RNA concentration was measured on a Nanodrop 2000.

Reverse transcription

Complementary DNA (cDNA) was reverse transcribed from the isolated RNA for each sample following the iScript Reverse Transcription Supermix kit instructions.

Single 20 µL reaction		Run protocol	
5x iScript Reaction Mix	4 µL	25ºC	5'
20x iScript Reverse Transcriptase	1 µL	46ºC	20'
RNA template	~300 ng	95ºC	1'
Nuclease-free water up to 20 µL		4ºC	∞

RT-PCR

Following cDNA synthesis, the expression load for the genes *FOSL1*, *EZH2*, *EED* and *SUZ12*, compared to *GAPDH* (Sup. Table 2; 7, 8, 9, 10, 11), in all samples was measured by RT-PCR. The IQ SYBR Green Supermix was kept in the dark and thawed on ice. Everything was briefly vortexed immediately before use. Primers were diluted to 10 µM working concentration and DNA templates were diluted 5x with nuclease-free water before use. Master mixes (MM) for each primer set were prepared of which 10 µL of each MM was added per well in a 96-well plate. 5 µL of diluted DNA templates were added separately to the wells in triplicates. After pipetting, a sticker lid was put on top of the plate and the plate was briefly centrifuged to collect all the liquids to the bottom of the wells and to remove bubbles. RT-PCR was performed on a RT PCR: CFX96 System.

Single 15 µL reaction		Run protocol	
5x IQ SYBR Green Supermix	7.5 µL	95ºC	3'
10 µM Forward primer	0.75 µL	95ºC	10''
10 µM Reverse primer	0.75 µL	60ºC	10''
Diluted DNA template	5 µL	72ºC	30''
Nuclease-free water	1 µL	Go To Step 2 39x	
		95ºC	10''
		65ºC	5''
		95ºC	5'

RT-PCR Analysis

Cq values of replicates with a greater difference of 0.4 were excluded from the analysis. Analysis was done according to the fold-difference method. First, the Cq values of *GAPDH* corresponding to each gene *FOSL1*, *EZH2*, *EED* and *SUZ12*, were averaged for each group individually. To obtain the delta Cq (dCq), from each sample Cq the corresponding averaged *GAPDH* value was subtracted. Then, the obtained dCqs were averaged for each group. To obtain the delta delta Cq (ddCq), the averaged dCq was subtracted from each individual dCq value. Then 2 to the power of the ddCq produced the fold difference. After calculating the fold difference, mean standard deviation and standard error were calculated for each group of folds, and loaded into GraphPad Prism to generate bar plots.

SDS-PAGE & Immunodetection

Protein isolation

After the siRNA experiment, protein lysates were extracted 48 hours after transfection, and following BRAF inhibition, proteins were collected after 72 hours. Organoids were released from the BME with dispase which was added at a final concentration of 1 mg/mL for 10' at 37ºC. After enzyme treatment, organoids were collected and washed with BM medium twice. Organoids were repelleted at 1800 RPM and the supernatant was aspirated. Cells were lysed with RIPA

lysis buffer supplemented with 1% protease inhibitors and 1:200 phenylmethylsulfonylfluoride for 30' on ice. Then samples were sonicated 3 x 5'' at the highest setting with 40'' breaks in between each sonication cycle. Following sonication, samples were centrifuged for 10' at 12.000 RPM at 4ºC. Supernatant containing the protein fraction was collected and stored at -80ºC.

Protein concentration

Following lysate preparation, protein concentration was measured with a Bradford assay. For this, the protein reagent dye concentrate was diluted 5x with sterilised water. To measure protein concentrations of the lysates, 2 µL of each vortexed lysate was mixed with 998 µL of the diluted dye. To generate a standard curve, bovine serum albumin (BSA) was mixed with the diluted dye:

BSA (1 mg/mL) µL	5x Diluted Dye µL
0	1000
2	998
4	996
6	994
8	992
10	990
15	985
20	980
30	970

Standard curve and sample absorbance were measured at 595 nm with a spectrophotometer.

Sample preparation

15 or 20 µg of protein lysate from each sample were mixed with RIPA lysis buffer. 5x sample buffer and boiled for 5' at 95ºC on a heat block immediately before loaded on the gels.

SDS-PAGE

Depending on their size, proteins were resolved either on 8% or 12% polyacrylamide gels via gel electrophoresis. Stacking gels were run at 100 V for 0.5 h and then running gels were run at 150-200 V until the front dye disappears at the bottom. Following electrophoresis, membrane transfer was performed using the Nitrocellulose kit and the Trans-Turbo Blot Transfer System. To ensure the proteins were successfully transferred to the membranes and were equally loaded in each lane, the blots were immersed in a Ponceaus solution for 5' at room temperature (RT) and then washed with DEMI water.

Immunodetection

Prior to immunodetection blots were immersed in 5% bocking solution (BSA x Tris-buffered saline 0.05% Tween-20 abbreviated as TBST) for 1 h at RT on a roller bank. Primary antibody solutions were mixed by adding antibodies against FRA1, p. FRA1, cMYC, p. cMYC, ERK, p. ERK, EZH2, EED, H3, H3K27me3, GAPDH, all raised in rabbit, 1:1000 in a 5% blocking solution overnight (o/n) at 4ºC. Primary antibody solution was collected and stored at -20ºC. The membranes were washed with TBST 4 times for 5' each on a roller bank. Secondary antibody solution was prepared by mixing anti-rabbit HRP antibody 1:1000 in a 5% blocking solution. The membranes were incubated with secondary antibody solution for 1 h at RT. The solution was aspirated and the membranes were washed with TBST 4 times for 5' on a roller bank. The proteins were visualised with the ECL Prime Western Blotting Detection Reagent Kit.

Imaging & quantification

Blots were imaged in an Amersham imager 600. With automatic exposure settings for chemiluminescence. Bands were analysed in Image Lab by using the Volume Tools → Rectangle → Local (subtraction method) → Analysis Table → Excel. The adjusted volume values were used to calculate protein expression. All different protein values were normalised to their corresponding GAPDH loading control bands and turned into percentages.

Chromatin immunoprecipitation RT-PCR

Primer design

Promoter regions of *EZH2*, *EED* and *SUZ12* genes where FRA1 and cMYC were previously shown to bind were identified in the hg19 UCSC Genome Browser with all Tracks activated for transcription factor binding and marks associated with active promoter. Genomic sequences with the strongest affinity, according to published literature on the website, for FRA1 and/or cMYC were picked for oligonucleotide design. Non-coding sequences where FRA1 and cMYC were do not bind were selected for background negative control. Each chosen primer sequence was copied and pasted in the Primer3 qPCR primer design engine. Sequence length was set between 50 and 150 bp and an average temperature of 65ºC. Primers were ordered from Integrated DNA Technologies or MERCK and reconstituted in Nuclease-free water to 100 µM upon arrival. Primer sequences are available in Supplementary Table 2 (1, 2, 3, 4, 5, 6).

RT-PCR

All reagents were briefly vortexed immediately before use. Primers were diluted to 10 µM working concentration, input DNA was diluted 50 times and immunoprecipitated DNA was diluted 2 times with Nuclease-free water. Primer sets 1, 3, 4, 6 and 2, 3, 5, 6 (Supplementary Table 2) were used for FRA1 and c-Myc RT-PCR reactions, respectively. Master mixes (MM) for each primer set were prepared of which 8 µL of each MM was added per well in a 96-well plate. 2 µL of diluted DNA templates were added separately to the wells in triplicates. After pipetting, a sticker lid was put on top of the plate and the plate was briefly centrifuged to collect all the liquids to the bottom of the wells and to remove bubbles. RT-PCR was performed on a RT PCR: CFX96 System.

Single 10 µL reaction	
5x IQ SYBR Green Supermix	5 µL
10 µM Forward primer	0.5 µL
10 µM Reverse primer	0.5 µL
Diluted DNA template	2 µL
Milli-Q	2 µL

Run protocol	
95ºC	3’
95ºC	15’’
60ºC	30’’
Go To Step 2 40x	
Melt curve:	
95ºC	1’
65ºC	5’’
95ºC	end

Input percentage

Results were analysed in Excel following an adapted version of the [93] protocol. Triplicate Cq values with a greater difference than 0.4 were excluded from the analysis. The raw Cq values were corrected for their dilution by calculating the log2 of the dilution factor (IN: log2 (2) = 1, IP: log2 (50) = 5.64) and subtracting it from the corresponding raw Cq value.

$$Cq\ (IN) = Cq\ (1\%\ IN) - log2\ (2)$$
$$Cq\ (IP) = Cq\ (50\%\ IP) - log2\ (50)$$

After adjusting for the dilution, the IN values of each group were averaged together and each IP value was subtracted from the corresponding averaged input. Then 2 was put to the power of the obtained number and multiplied by 100.

$$\Delta Cq = Cq\ (IN) - Cq\ (IP)$$
$$Percentage\ of\ Input = 2^{\Delta Cq} \times 100$$

3D sprouting assay

Sample preparation

The sprouting assay was adapted from Koorman et al., 2022. Organoids were collected from BME using 1 mg/mL dispase for 10’ at 37ºC. Organoids were collected in 15 mL falcon tubes and washed twice with BM. Then they were pelleted at 1800 RPM and supernatant was discarded. The organoids were resuspended in BM and seeded at ~250 organoids per 2.5 µL of suspension for each group. Counting was done with a mechanical tally by eye on an EVOS stereomicroscope. 2.5 µL of each cell suspension were mixed with 7.5 µM either neutralised Collagen I (see next section) or BME and seeded onto polymer-bottom 5-well plates in 10 µL droplet per well. The seeded matrix droplets were polymerised for 1-2 hours at either physiological 37ºC or 26ºC for larger pore formation to promote collective invasion, as per personal advice from Koorman et al’s writers [91]. Pre-warmed BM (low serum/growth factor) media was added 45 µL per well. In an experiment involving BRAF inhibitors

encorafinib and vemurafinib, were added to a final concentration of 1 µM and to T10 and NC. For a negative control, equal to the drugs in microliters of Dimethyl sulfoxide (DMSO) were added to all lines T10, NC, BC1 and BC2.

Collagen I preparation

Collagen I was handled on ice and buffers were pre-chilled to prevent pre-polymerisation. Collagen I from rat tail was neutralised with 1M NaOH to pH 7.0 – 7.5 with the help of pH strips. Neutralised collagen was diluted to 2 mg/mL final concentration with PBSx1.

Quantification

The organoids were imaged daily with an EVOS stereomicroscope. Sprouting and cells that were separated from the organoids were manually counted in Image J (FIJI) using Plugins → Analyze → Cell counter. The number of sprouting was normalised to the total number of organoids within the same field.

Immunofluorescence

48 hours after seeding, organoids were fixed in 4% Paraformaldehyde for 1.5 h, followed by permeabilisation with PBD0.2T (Triton X-100 0.2%, Bovine Serum Albumin 1%, DMSO 1%, dissolved in PBSx1) buffer. Primary antibody against CK20 (mouse, 1:500) was mixed in PBD02 and added overnight. The next day, wells were washed three times for 5' with PBD.02T on a shaker. Then, secondary antibody anti-mouse Alexa Fluor 647 (5 µg/mL), nuclear stain DAPI (1:1000) and Collagen I probe CNA35-GFP (1:1000), were mixed into the PBD0.2T buffer and added to the organoids for 2 hours in the dark on a shaker. Following secondary antibody staining, the wells were washed with PBD02 three times for 5' in the dark on a shaker. Then the organoids were mounted with one droplet per well with mounting medium.

Microscopy & image analysis

Mounted organoids were imaged on a confocal microscope Zeiss LSM 700 at 40x magnification. Z-stacks of organoids from each group were made following the default Zen Zeiss software settings. Then, Z-stacks were saved as ome.tifs and processed in Image J (FIJI). Ome.tif files were opened as colorised hyperstacks in Image J. Then a 3D projection was made following Plugins → 3D Viewer or Image → Stacks → 3D project.

Results

Sequencing results of CRC organoid lines confirmed that T10 and NC are heterozygous for the *BRAF*-V600E mutation and BC1 and BC2 were *BRAF*-wt (data not shown).

Protein expression analysis of *BRAF*-V600E mutant and *BRAF*-corrected colorectal cancer organoids treated with BRAF or FRA1 inhibitors.

Phosphorylation of ERK, cMYC and FRA1 are BRAF-dependent

To validate that FRA1 is directly regulated by the MAPK pathway, we used encorafenib and vemurafenib specific BRAF inhibitors or DMSO (control) on *BRAF*-V600E mutant CRC organoid lines (T10, NC), and compared them to DMSO-treated lines. Following drug treatment, immunoblotting revealed protein levels of cMYC and phosphorylated cMYC were decreased compared to DMSO-treated *BRAF*-mutant lines, and were comparable to the expression of *BRAF*-corrected clones (Fig. 3). CMYC being a known target of MAPK signalling, confirms that the BRAF blockade was successful [92]. This is also evident by the decrease in phosphorylation of ERK in *BRAF*-V600E mutants, by encorafenib and less by vemurafenib (Fig. 3). However, the chemo-drugs could not lower phosphorylation of ERK to BRAF-wt levels (Fig. 3). Similar pattern of downregulation as to phosphorylated ERK was observed in FRA1, although on a lower scale. Expression of FRA1 and its phosphorylation were more decreased by encorafenib than by vemurafenib in the T10 mutant line, compared to DMSO-treated mutants (Fig. 3). FRA1 expression was absent in BC clones and completely diminished in BRAF-inhibitor-treated mutants (Fig. 3). Phosphorylation of FRA1 was comparable between corrected clones and drug-treated NC. Overall, the inhibition of BRAF successfully decreased the phosphorylation of ERK that in turn downregulated FRA1 expression and phosphorylation to *BRAF*-wt levels, confirming previous statements that FRA1 is directly regulated by the MAPK pathway (Sup. Fig. 2, D, E) Gruda et al., 1994; Terasawa et al., 2003; Treinies et al., 1999).

Expression of PRC2 core component proteins are not BRAF-dependent

EZH2 and EED expression had no discernible pattern between different treatments or lines (Fig. 3). According to the quantification, EED expression was decreased in vemurafenib-treated T10, but that is not clearly visible on the blot (Fig. 3). The H3K27me3 is predominantly methylated by EZH2 and thus should follow a similar expression pattern, however, H3K27me3 was variable and independent of BRAF status (Fig. 3). Histone H3, being one of the core proteins in chromatin should be equally expressed regardless of post-translational modifications and therefore was included as a control to H3K27me3, but it showed differential expression, except for in *BRAF*-corrected clones where H3 was consistent (Fig. 3) [94]. The variation in H3 could be underlying the variable expression of the H3K27me3 mark. These results show that there was no effect of BRAF inhibition on any of the PRC2 components, and the outcome is inconclusive for H3 and H3K27me3. In comparison, although not detected by quantification, the blots had visibly lower levels of EZH2 and EED in the *BRAF*-corrected lines, but not completely absent, indicating that EZH2 and EED maintain expression in *BRAF*-wt (Fig. 3). The H3K27me3 was not present in the *BRAF*-corrected clones that stably expressed H3, suggesting that in *BRAF*-wt the EZH2 protein is expressed but is not enzymatically active.

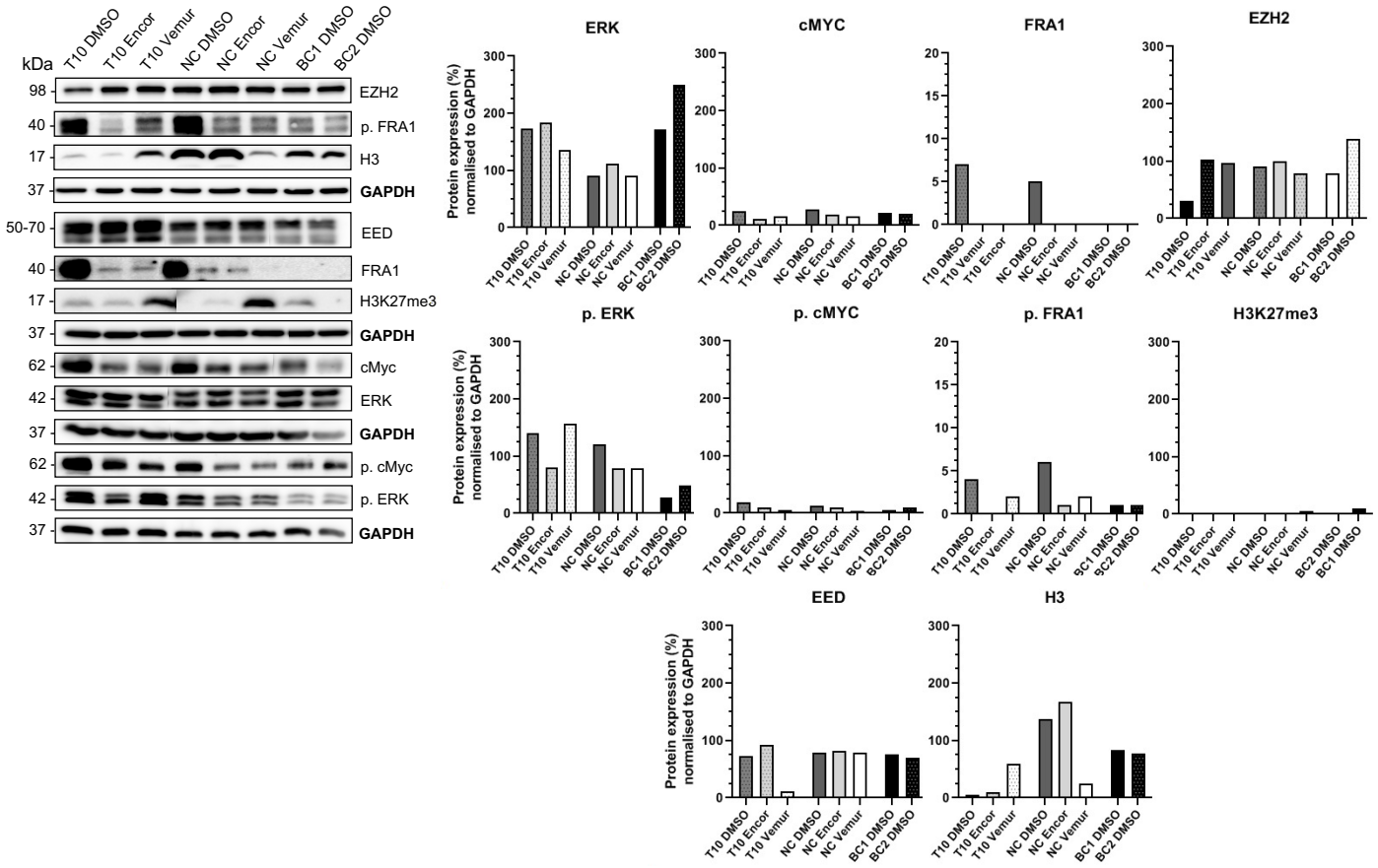

Figure 3. Protein expression comparison between *BRAF*-V600E and *BRAF*-corrected colorectal cancer organoids with or without BRAF inhibitors.

BRAF-V600E mutant (T10, NC) and *BRAF*-corrected (BC1, BC2) CRC organoid lines were treated immediately after cell seeding. DMSO was used as a negative control to all lines. Each *BRAF*-V600E line was treated with encorafenib (Encor) and vemurafenib (Vemur) BRAF inhibitors individually. Protein lysates were collected 72 hours after the drugs were added and were detected via immunoblotting. The immunoblots as representative and were imaged with an Amersham Imager 600 imaging system. Protein bands were analysed in ImageLab and each sample was normalised to its corresponding GAPDH loading control band (N=1). Graphs were generated using GraphPad and represent protein quantification.

Expression of PRC2 core components is not FRA1-dependent

To identify if PRC2 core genes are affected by FRA1 in relation to the V600E overactivation of BRAF, we used small interfering RNA to block transcription of *FOSL1* (siFOSL1) and negative control siCntrl. We compared

mRNA and protein expression between siFOSL1-treated and siCntrl-treated *BRAF*-V600E CRC organoid lines. Gene expression analysis revealed that *FOSL1* was lowered by 0.5-fold and increased by 0.5-fold upon *FOSL1* inhibition in T10 and NC, respectively (Fig. 4, A). On a protein level FRA1 was almost completely diminished and its phosphorylation was also decreased after siFOSL1 addition in both organoid lines, contradicting the *mRNA* expression in NC (Fig. 4). Following siFOSL1 treatment, *mRNA* expression of all PRC2 core genes was slightly decreased in both lines, except for *EED* which was upregulated in T10 (Fig. 4, A). These results are reflected by the western blots that show no effect of FRA1 inhibition on EZH2 and EED in NC, and a slight decrease of EZH2 in T10 (Fig. 4). Total cMYC and phosphorylated cMYC were unaffected by *FOSL1* depletion in both lines (Fig. 4, B). Total ERK and phosphorylated ERK remained the same in siFOSL1 and control treatment in T10. In NC, total ERK levels were also unaffected, phosphorylated ERK was 100 times more upregulated compared to the rest of the proteins in control-treated, and relative to the siFOSL1-treated (Fig. 4, B). H3 was increased in both NC and T10 treated with siFOSL1 compared to controls. H3K27me3 show contradicting results whereby protein expression is enhanced in siFOSL1-treated T10 and diminished in NC (Fig. 4, B). Even though the FRA1 protein expression changes are not reflected on *mRNA* level in NC, there is a visible decrease in FRA1 and p. FRA1 in FRA1-inhibited wells, indicating that the siRNA treatment was partially effective in downregulating the transcription of *FOSL1* and thus translation of FRA1, and that no effect on EED, EZH2 and H3K27me3 was observed. We cannot exclude the possibility that the effect of siRNA was insufficient to reach possible targets of FRA1 due to, for example, short exposure or low transfection efficiency. In contrast to the previous blot in Figure 2, H3 was consistent between all lines and treatments (Fig. 4, B). As cMYC is not a target of FRA1 it was not expected to be affected by FRA1 levels, and that is reflected by the homogenous cMYC expression and phosphorylation between controls and siFOSL1-treated (Fig. 4, B).

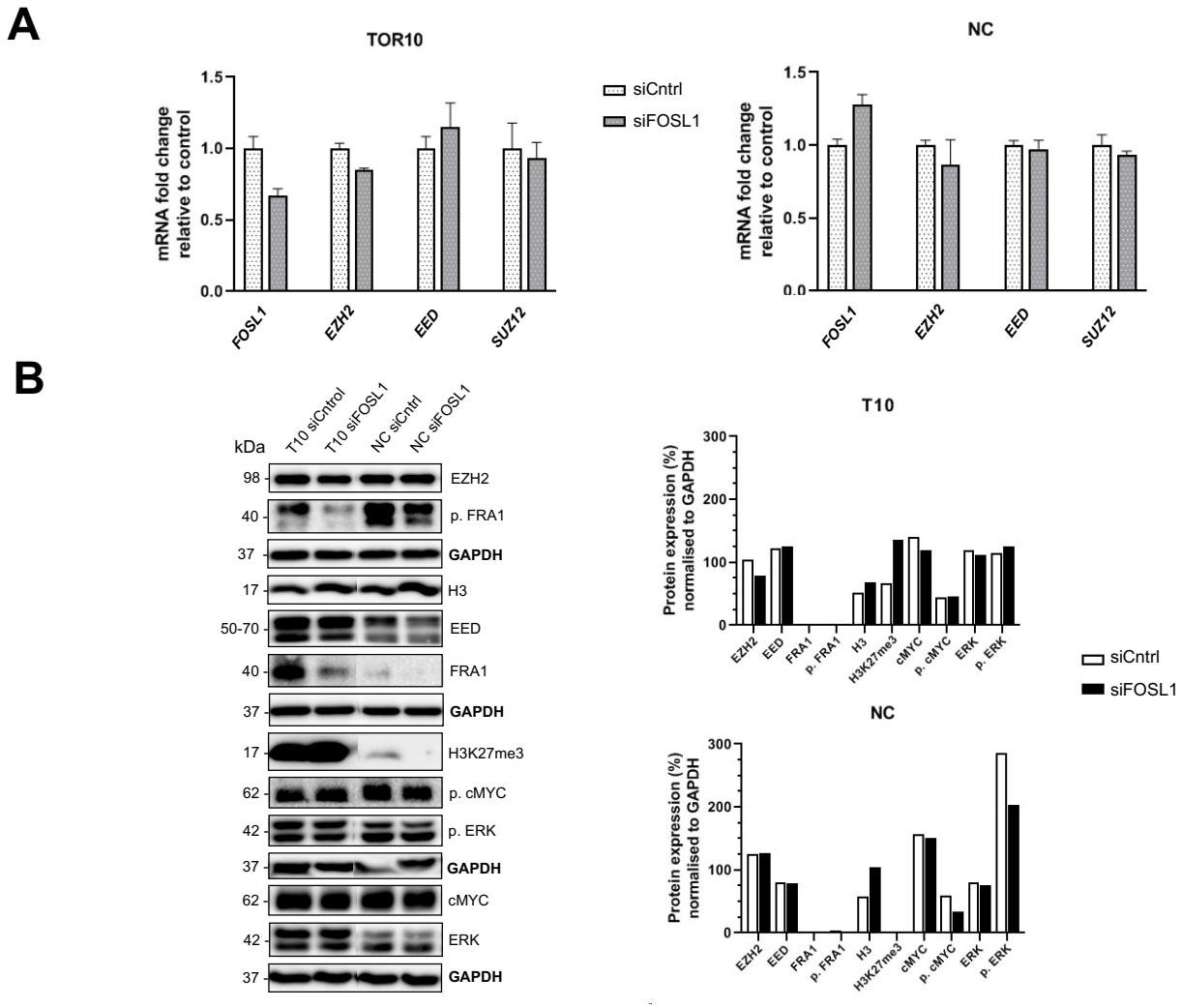

Figure 4. *MRNA* and protein expression comparison between *BRAF*-V600E and *BRAF*-corrected colorectal cancer organoids with or without small interfering RNA against *FOSL1*.

(A) *BRAF*-V600E organoids (T10, NC) were treated with either negative control siCntrl or siFOSL1 against *FOSL1* transcription (N=1). *MRNA* was collected 24 hours after treatment and reverse transcribed into cDNA. RT-PCR using the cDNA as template was carried out to measure the expression of *EZH2*, *EED* and *SUZ12* genes. The fold difference between the genes was calculated by normalising siFOSL1-treated samples to controls.

(B) Protein lysates were collected 48 hours after siRNA treatment and proteins were immunoblotted. The blots were imaged with an Amersham Imager 600 Imaging System and protein bands were analysed in Image Lab. Protein expression of each sample was normalised to its corresponding loading control GAPDH represented by graphs generated in GraphPad.

Morphological phenotype analysis of *BRAF*-V600E and *BRAF*-corrected colorectal cancer organoids in two types of tissue matrices

Collagen I promotes sprout formation in BRAF-V600 mutants

To understand the effect of the *BRAF*-V600E mutation on organoid morphology, we used *BRAF*-V600E and *BRAF*-corrected clones in a metastatic promoting setting using Collagen I and compared it to the Collagen IV-rich BME matrix. In standard conditions of BME, organoids, regardless of *BRAF* status formed spherical structures with a similar cystic morphology with occasionally visible apical lumen (Fig. 5, A).

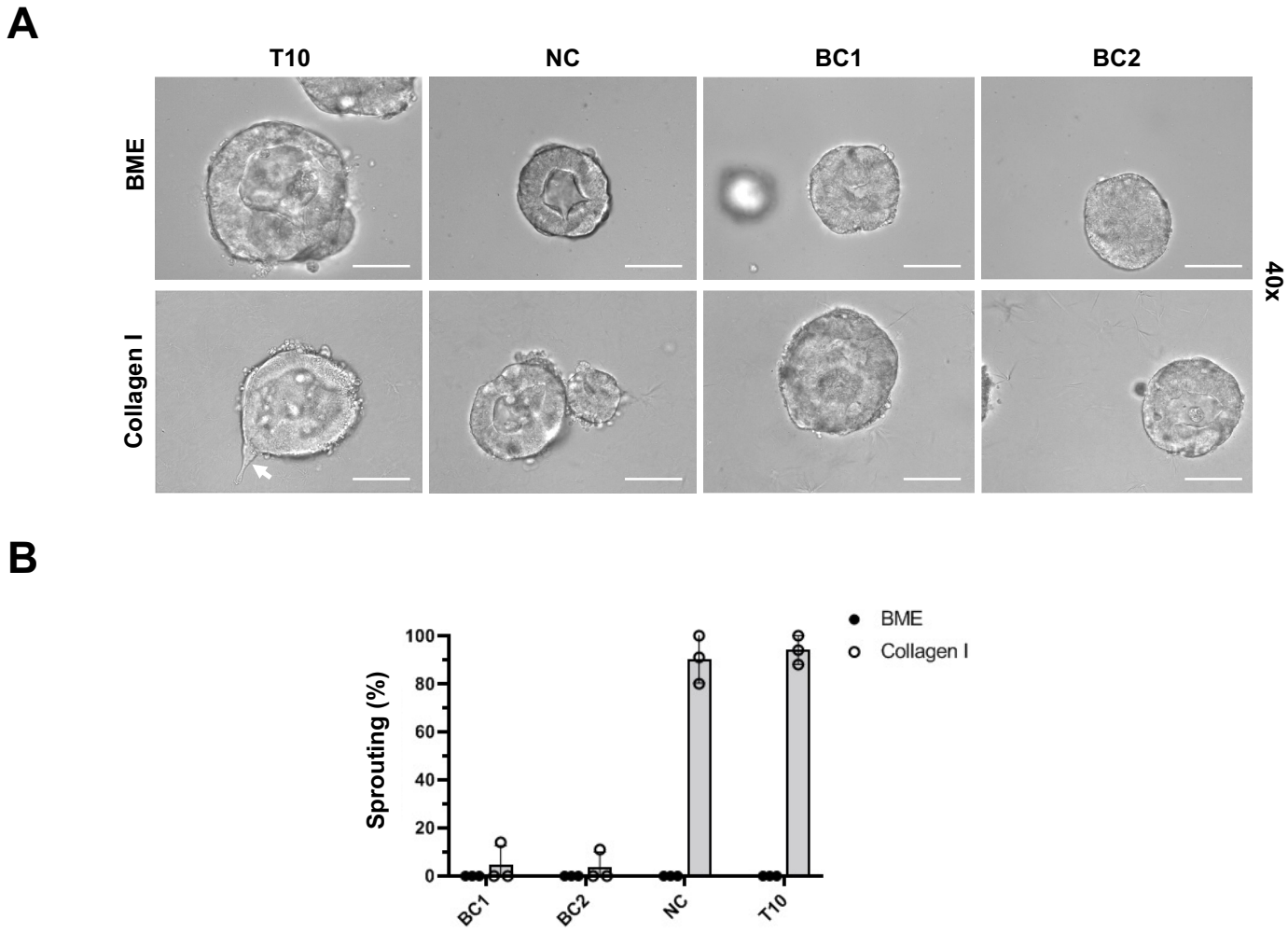

Figure 5. Morphological phenotype and quantification of *BRAF*-V600E mutant and *BRAF*-corrected colorectal cancer organoids in BME or collagen I matrices.

(A) *BRAF*-mutant (T10, NC) and *BRAF*-corrected (BC1, BC2) clones were seeded in either BME or Collagen I (N=1). Images were taken with a stereomicroscope (EVOS) 48 hours after cell seeding and are representative. The white arrow marks a sprouting event. Magnification is 40x and scale bar is 50 µm.

(B) Sprouting was quantified by counting all organoids with sprouts and normalising it to the total number of organoids within the same field (N=1). Images of multiple wells of the same group were treated as technical repeats. Graphs were generated in GraphPad, error bars represent standard deviation.

No morphological differences were identified between *BRAF*-corrected clones cultured in BME and Collagen I (Fig. 5). However, lines carrying the *BRAF*-V600E mutation displayed an aberrant morphology in Collagen I whereby individual or more cells formed protrusions pointed outward to the extracellular matrix also referred as sprouts (Fig. 5, A). Quantification revealed that mutant organoids formed sprouts at ~90% in Collagen I, but not in BME, and *BRAF*-wt lines did not have differences in morphology in either condition (Fig. 5, B). These results indicate that Collagen I promotes morphological changes in the *BRAF*-V600E mutants, but these changes are not observed in a normal Collagen IV-rich BME matrix. This suggests that the *BRAF*-V600E mutation induces molecular events that result in the acquired ability of organoids to deform in a metastatic-mimicking environment.

Cell protrusion formation could be inversely related to cell separation in time

To gain a better understanding of sprout formation dynamics we followed the morphology of the *BRAF*-V600E mutant T10 line for three days in BME or Collagen I. In an attempt to prevent possible cell death from anoikis we included ROCK inhibitor and compared it to non-treated organoids. In addition to sprouting, another phenotype was identified, characterised by cells that appear to detach from the organoids in Collagen I, referred as dissemination (Fig. 6, A). On the day of organoid seeding, there is nearly 100% sprout formation in Collagen I, that decreases with 20% on the following days, regardless of ROCK inhibitor (Fig. 6, B). The opposite trend was observed whereby disseminating cells or cell debris increase from almost none to between ~70% on the second day in Collagen I (Fig. 6, B). Furthermore, there is 20% more cells that were separated from the organoids with the addition of ROCK inhibitor in Collagen I on day 2 (Fig. 6, B), indicating that the detached cells might survive better with the drug. Although ROCK inhibitor is a potent inhibitor of death from cell detachment, it does not prevent cells from dying by other factors [95]. However, we did not perform specific assays to confirm if the separated cells were dead or alive, and therefore we can only speculate. No sprouting events and a 20% increase in dissemination on the first day were observed in BME +/- ROCK inhibitor (Fig. 6, B). These results confirm that the *BRAF*-V600E mutation leads to sprout formation in a Collagen I matrix regardless of ROCK blockade, but more in-depth research is required to understand the condition of the detached cells.

BRAF inhibition reversed the sprouting morphology in a Collagen I matrix

We used immunofluorescent staining to gain a deeper insight into sprouting events in *BRAF*-V600E mutant (T10, NC) compared to *BRAF*-corrected (BC1, BC2) CRC and healthy colorectal (H040-N) organoids. We used specific BRAF inhibitors in an attempt to reverse the sprouting phenotype. CK20 is an epithelial marker, characteristic for cells of the intestinal mucosa, and is outlining the basolateral and apical membranes of the CRC organoids (Fig. 7, A). Neither of the organoids in BME formed sprouts, and *BRAF*-corrected and healthy lines did not form protrusions in Collagen I (Fig. 7). The healthy H040-N presented with abnormal formation of multiple luminae and a sheet-like spread-out flattened morphology. The sheet-like morphology is reminiscent of epithelial cell lines (e.g., Caco-2) in 2D culture conditions where they form a polarised monolayer of epithelium and also of the simple epithelium adjacent to the mesoderm *in vivo* [96,97]. This suggests that the organoids derived from a non-cancerous tissue 'behave' like normal epithelium and form continuous sheets, rather than 3D spheres, regardless of matrix composition (images for H040-N in BME not shown). The appearance of multiple luminae could be a consequence of the flattened formations, as opposed to the well-described intestinal self-assembling intestinal spheroids that form a single apical lumen [98]. After 2 days in Collagen I, T10 and NC displayed ~80% and ~40% of protrusions, respectively. Protrusions seem to follow the shape of the collagen crimping as they are formed in the same direction as the collagen bundles (Fig. 7, A). Encorafenib decreased sprouting by 1/2 and vemurafenib – by 1/3 in T10 by the end of treatment in Collagen I, whereas BRAF inhibitors completely abolished sprout formation in NC (Fig. 7). Overall, these results further solidify previous findings that *BRAF*-V600E is responsible for protrusion formations in a Collagen I matrix, that could be reversed with inhibition of the BRAF kinase.

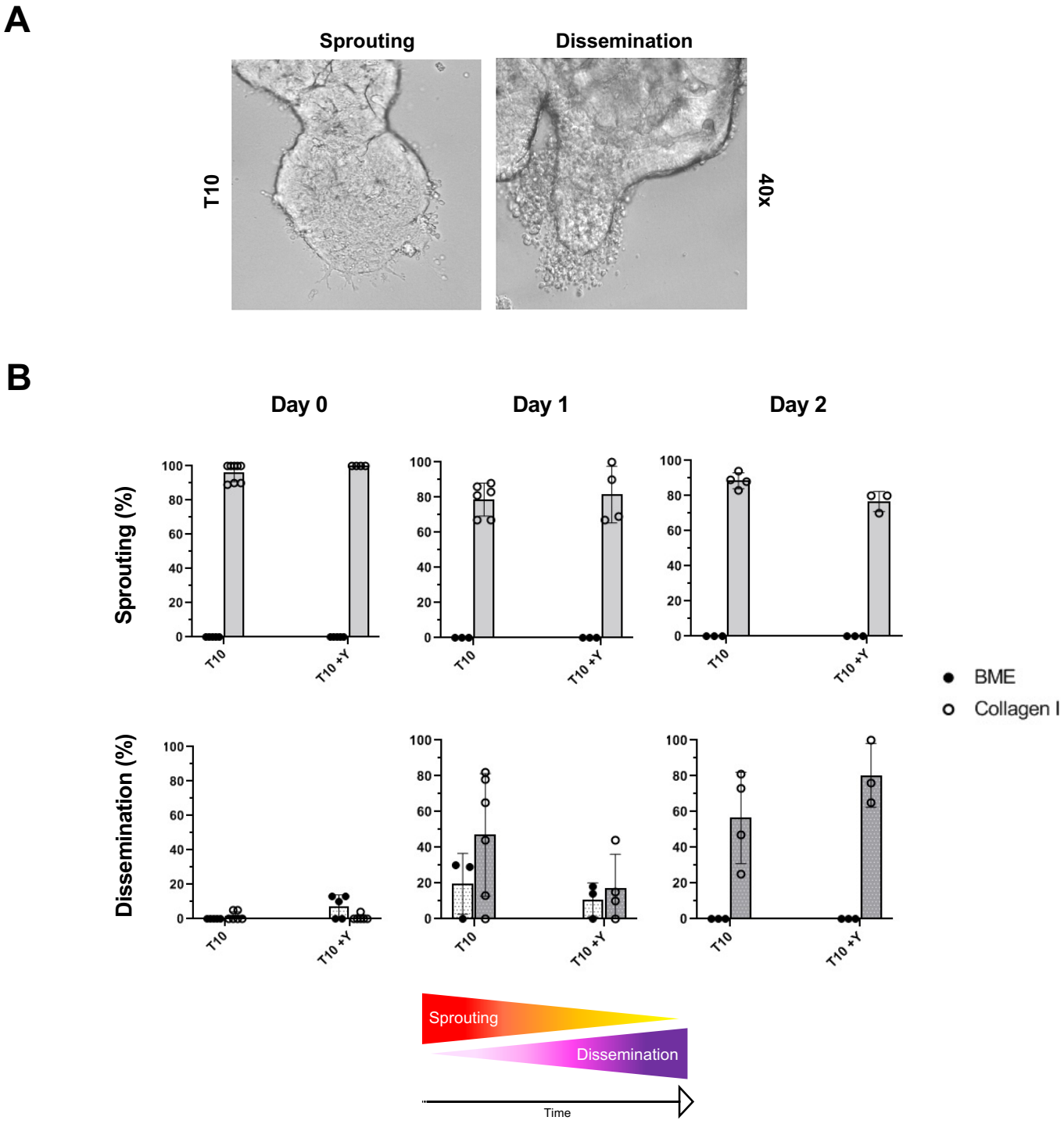

Figure 6. Morphology and quantification of sprouting and dissemination of a *BRAF*-V600E mutant colorectal cancer organoid line in Collagen I with or without ROCK inhibitor.

(A) Images were generated 24 hours after cell seeding and are representative of sprouting and dissemination morphology. Magnification is 40x and scale bar is 50 µm.

(B) The organoids were imaged daily for 3 days using a stereomicroscope (EVOS). Both sprouting and dissemination were quantified by counting all organoids with sprouts and with separating cells and normalising it to the total number of organoids within the same field (N=1). Images of multiple wells of the same group were treated as technical repeats. Graphs were generated in GraphPad, error bars represent standard deviation.

A

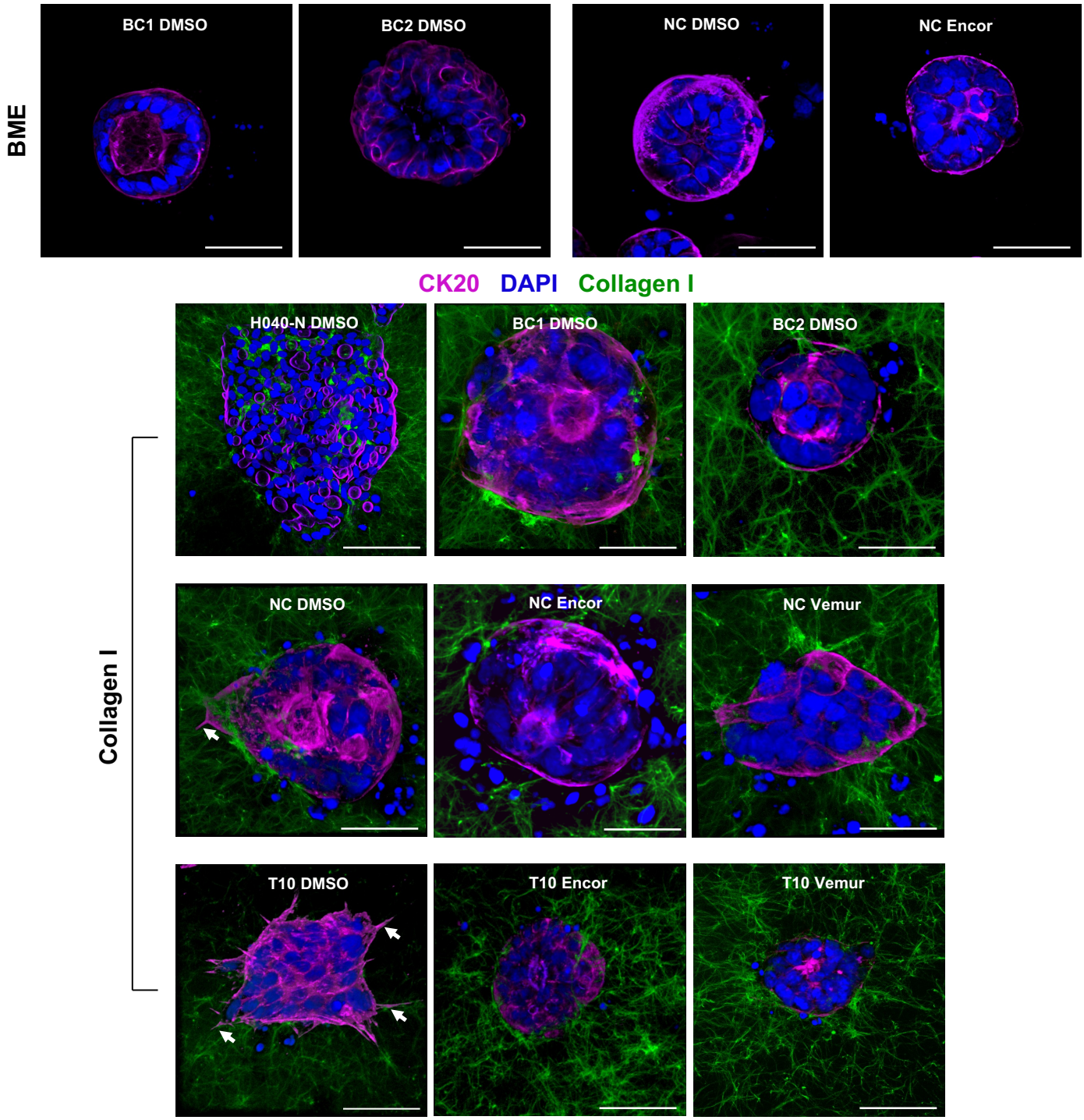
BME
BC1 DMSO
BC2 DMSO
NC DMSO
NC Encor
CK20 DAPI Collagen I
Collagen I
H040-N DMSO
BC1 DMSO
BC2 DMSO
NC DMSO
NC Encor
NC Vemur
T10 DMSO
T10 Encor
T10 Vemur

B

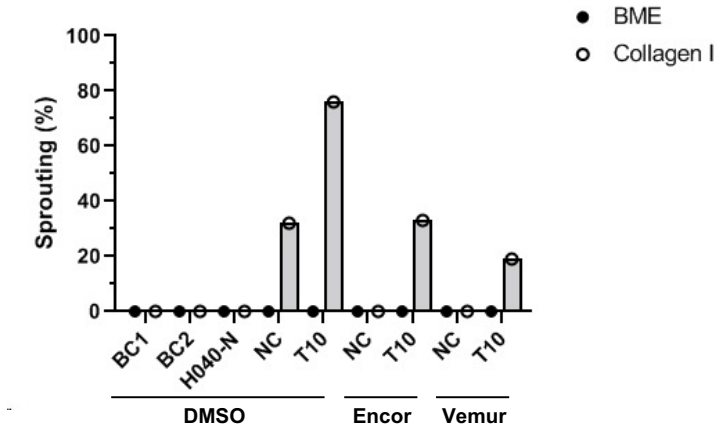
BME
Collagen I
Sprouting (%)
100
80
60
40
20
0
BC1
BC2
H040-N
NC
T10
NC
T10
NC
T10
DMSO
Encor
Vemur

Figure 7. Immunofluorescent staining and quantification of sprouting morphology of *BRAF*-V600E mutant, *BRAF*-corrected colorectal cancer and healthy colorectal organoids in BME or Collagen I with or without BRAF inhibitor.

(A) Organoids from all groups were seeded in either BME or Collagen I, and the matrices were polymerised at 26ºC (N=1). After polymerisation, *BRAF*-V6600E lines (T10, NC) were supplied with BRAF inhibitors or DMSO, and *BRAF*-corrected (BC1, BC2), non-mutant colorectal organoids (H040-N) were treated only with DMSO as a negative control. Organoids were fixed 48 hours after seeding and immunofluorescently labelled for cytokeratin 20 (CK20) in magenta, nuclear DAPI in blue and Collagen I in green. Images were generated with a Zeiss LSM 700 confocal microscope at 40x magnification and scale bars are 100 µm. Images of T10 and H040-N in DMSO BME were not included due to the files being corrupt.

(B) Images of organoids were obtained with a stereomicroscope (EVOS) 48 hours after treatment and before fixation for immunofluorescence. Sprouting was quantified by counting all organoids with sprouts which was normalised to the total number of organoids within the same field.

FRA1 promoter occupation of PRC2 core genes

To understand the molecular involvement of FRA1 with the PRC2 core genes, DNA from *BRAF*-V600E and *BRAF*-corrected lines was immunoprecipitated for the presence of FRA1 and that was compared to non-immunoprecipitated (input) DNA. Using specific primers for the promoters of *EZH2*, *EED*, *SUZ12* and negative control background regions, we performed RT-PCR to identify enrichment of FRA1, compared to cMYC, in those regions in both immunoprecipited and input DNA.

Primer efficiency and target specificity

The quality of primer sets was assessed from the melt curve of the RT-PCR reaction. Both *EZH2* primer sets I and II displayed unstable melt curves with two peaks indicating that the primers amplify two targets in immunoprecipitated and input DNA samples (Fig. 8, A, EZH2 I, EZH2 II). Peak height and number are indicative of primer affinity and specificity, respectively, therefore we can conclude that *EZH2* primers were not specific and cannot be used for further analysis. Cq values are inverse to the amount and copies of the target DNA in a sample and are registered in the exponential phase of DNA amplification above the threshold line. Lower Cq values (<29 cycles) indicate higher amounts of the target nucleic acid, and vice versa, higher Cq values (>38 cycles) indicate lower amounts of the target sequence [99]. Since background primers were designed to amplify a non-coding region where FRA1 and cMYC do not bind, they were expected to not amplify above the threshold line in either immunoprecipitated or input DNA. However, the signal from the background primers in all cases reached above the threshold early between the 10th and the 20th cycle, and formed multiple peaks (Fig. 8, A). Early rise in amplification can indicate formation of primer dimers, rather than oligonucleotides binding to the DNA. Although, they are not expected to bind to any DNA, the primers should remain under the threshold level. Therefore, due to possible primer-dimer formation the background oligonucleotides were deemed unreliable. EED primers reached saturation at 26 cycles for the input DNA and at 30 cycles for the immunoprecipitated DNA in both cMYC and FRA1, and formed single high peaks indicative of specific primer binding with strong affinity for the region of interest (Fig. 8, A). The SUZ12 I primer set amplified its target in input and FRA1-pulled DNA between 28 and 30 cycles, respectively, but formed a smaller peak in addition to the big peak of the peak curve. The smaller peak can indicate unspecific binding or different melting temperatures of that specific DNA region and/or of oligonucleotides. The SUZ12 II set amplified the input DNA after 34 cycles, and the cMYC-DNA after 40 cycles, but did not form peaks (Fig. 7, A). As mentioned before, higher Cq corresponds to lower amount of target DNA, or poor oligonucleotide design or low enrichment of cMYC at the SUZ12 promoter.

FRA1 does not occupy promoters of PRC2 genes in a BRAF-dependent manner

FRA1 was shown to bare binding sites for *EZH2* and ChIP revealed that FRA1 indeed occupies the *EZH2* promoter in cell lines that have an intrinsic higher expression of FRA1 [84]. Moreover, dysregulations in either FRA1 or EZH2 have been found to have overlapping molecular and morphological changes in cancer [84,100]. Therefore, we hypothesised that FRA1 could promote these changes via the PRC2 complex through *EZH2*, and possibly through interaction with the other core components *EED* and *SUZ12*. As FRA1 is stimulated in *BRAF*-V600E mutants (Sup. Fig. 2), we expected to observe increased FRA1 occupancy on PRC2 promoters in the mutant organoid lines. However,

due to poor oligonucleotide design and technical challenges of the RT-PCR assay, we could not make any conclusions about FRA1 and cMYC enrichment at the *EZH2* and *SUZ12* promoters. FRA1 was not detected at the EED promoter in a *BRAF*-dependent manner, as NC-mutant and BC1-corrected lines showed similar values (Fig. 8, B). Although the data for *EZH2* and *SUZ12* is unreliable, similar outcome to *EED* was observed in the rest of the genes, but we could only assume that FRA1 was not enriched at PRC2 promoters in *BRAF*-V600E mutants compared to *BRAF*-wt (Fig. 8). It seems that cMYC was more enriched in *BRAF*-mutants compared to *BRAF*-corrected lines, however, we were faced with multiple technical challenges along with unspecific primer amplification that prevented us from extracting any definitive conclusion about cMYC at PRC2 promoter regions (Fig. 8).

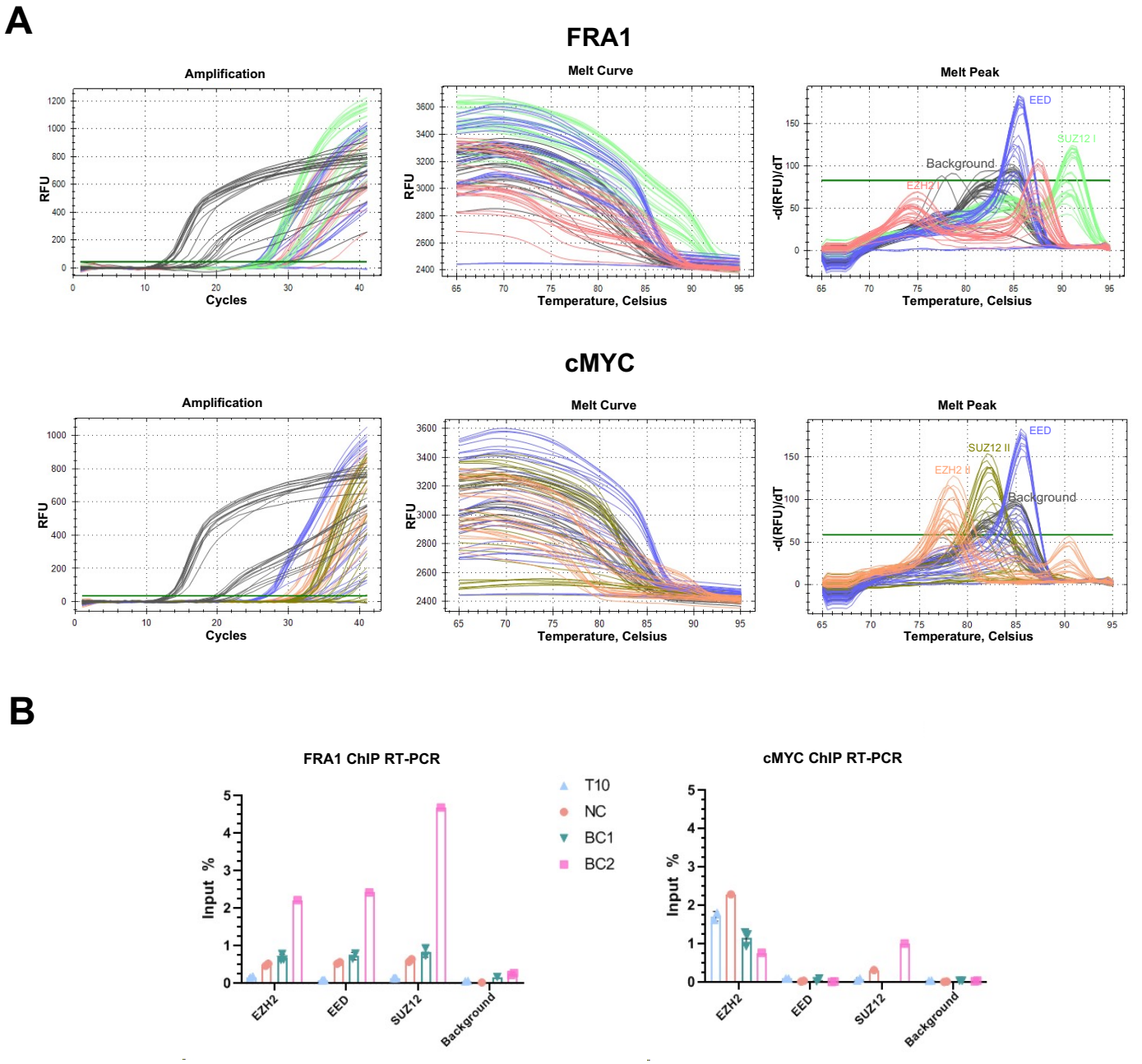

Figure 8. Primer efficiency and FRA1 enrichment at PRC2 core promoter regions in *BRAF*-V600E mutant vs *BRAF*-corrected DNA using chromatin immunoprecipitation RT-PCR.

DNA from *BRAF*-V600E mutant (T10, NC) and *BRAF*-corrected (BC1, BC2) lines was crosslinked to DNA-bound proteins and immunoprecipitated with antibodies against either FRA1 or cMYC, the latter used as a positive control for transcription factor enrichment at promoters. Non-immunoprecipitated DNA was used as input control and is characterised by an earlier amplification above the threshold line at 0 and higher melt peaks compared to immunoprecipitated DNA (A). Background represents regions of the DNA that FRA1 and cMYC should not occupy. Both the immunoprecipitated and input DNA were used as templates for a RT-PCR reaction.

(A) Following RT-PCR, primer efficiency was determined by the amplification and melt curves, and primer specificity was estimated using the melt peaks. Different primer sets are displayed in different colours: EZH2 I (pink), EED (purple), SUZ12 I (green), Background (Black), EZH2 II (orange), SUZ12 II (dark green).
(B) Input percentage represents the DNA pulled down by FRA1 or cMYC antibody relative to the input DNA and shows the enrichment of FRA1 or cMYC at the *EZH2*, *EED* and *SUZ12* promoters. Error bars represent standard deviation.

Discussion

The *BRAF*-V600E mutation was shown to be more potent in upregulating the MAPK pathway compared to other activating mutations (e.g., in *KRAS*) and is associated with low survival and poor response to anti-EGFR chemotherapy drugs in metastatic CRC [47–49,101,102]. In a research to find differentially expressed targets of the MAPK pathway, the Kranenburg group identified that *FOSL1* was upregulated in *BRAF* mutants compared to *KRAS* in CRC organoids (Sup. Fig. 1, A). Further analyses in CRC-derived organoids and patient biopsies revealed that the *FOSL1* gene was preferentially upregulated in *BRAF* mutant compared to *BRAF* wild type samples, in agreement with analysis of the large TGCA cohort (Sup. Fig. 1, B, C). More specifically, *FOSL1* and its target genes were preferentially upregulated in *BRAF*-V600E CRC organoids compared to *BRAF*-corrected (Sup. Fig. 2, A-C). Furthermore, previous evidence that FRA1 is regulated by ERK-mediated phosphorylation, was confirmed by targeting the BRAF kinase [58,60,62]. Consequently, ERK was not phosphorylated, and this prevented overall FRA1 expression and phosphorylation, confirming that FRA1 is downstream of MAPK, and tightly regulated by BRAF (Sup. Fig. 2, D, E). There is strong evidence that implicates *FOSL1* in various aspects of the metastatic cascade in different cancers. *FOSL1* differential expression is highly associated with gene panels responsible for invasion (matrix-degrading enzymes, integrins, cytoskeletal rearrangements) and stemness (proliferation, evading cell death from anoikis) [70,78,83,84,100]. Earlier it has been shown that FRA1 is dispensable for cell proliferation, but essential for metastasis in CRC *in vitro* and *in vivo* [71,74]. The exact role of FRA1 in metastasis is unclear, however, there is evidence that it could be through interaction with *EZH2*, a known driver of EMT and stemness [70,103]. It was shown that the major methyltransferase of the PRC2 complex, *EZH2* has binding sites for FRA1 which is indicative of FRA1-mediated regulation [84].

Since *FOSL1* is preferentially upregulated in the *BRAF*-V600E mutation, and is involved in metastasis, we hypothesised that *FOSL1*/FRA1 could play an important role in promoting molecular and morphological changes that are beneficial for the progression of malignant CRC. To test this, the *BRAF*-V600E-positive CRC was modelled with the use of patient-derived *BRAF*-V600E mutant and *BRAF*-corrected organoid lines. We tested the effect of the *BRAF*-V600E mutation in combination with a metastatic-promoting environment on organoid morphology. Anti-cancer drugs that target BRAF were tested if they can efficiently reverse the molecular and morphological changes induced by the *BRAF*-V600E mutation. To better understand the downstream molecular events of FRA1, we specifically targeted *FOSL1* transcription and we analysed FRA1 interaction with promoters of PRC2 core genes known to be important for maintaining a stem-cell like state and EMT.

By targeting BRAF, we partially depleted p. ERK which in turn downregulated FRA1 and p. FRA1, confirming previous findings that FRA1 is regulated by the MAPK cascade and that FRA1 is overexpressed specifically due to the *BRAF*-V600E mutation [50,62]. The BRAF inhibition is also reflected by the downregulation of cMYC and p. cMYC which are downstream of BRAF (Fig. 3). We used cMYC as an additional control for the BRAF inhibition, as cMYC is partially regulated by the MAPK cascade. In *BRAF*-V600E-mutants cMYC and p. cMYC were downregulated to *BRAF*-wt levels, following BRAF inhibition, further confirming the treatment was successful. Since the PRC2 complex is known to be downstream of BRAF signalling and partially regulated by BRAF-effectors, including cMYC, we expected to see a downregulation of the core proteins EZH2 and EED, upon a BRAF blockade. Although FRA1 and cMYC were successfully decreased we did not observe any changes in the PRC2 gene products. We established that EZH2 and EED maintained protein expression under *BRAF*-wt, however, it was lower compared to the expression in *BRAF*-V600E mutant and compared to drug-treated organoids. This indicates that the effect of the drugs was too transient to produce a significant difference in downstream targets of cMYC and possibly of FRA1. The efficiency of inhibition is highly dependent on the duration of the drug treatment, the timing of protein collection and the half-life of the drug. The half-life of encorafenib is >30 hours *in vitro* and vemurafenib is cleared after ~57 h *in vivo*, which is likely decreased *in vitro* [104,105]. In addition, in comparison to encorafenib,

vemurafenib is known to have a more transient inhibitory effect according to unpublished studies of the Kranenburg group. In our case, the inhibitors were added once and proteins were collected 72 hours later, allowing the drugs to get completely cleared and therefore replenish BRAF signalling. It has been previously shown that encorafenib was sufficient to deplete cMYC expression and phosphorylation, but after 16 hours expression was renewed (Sup. Fig. 2, E). Therefore, we can argue that the effect of the drugs was initially stronger, but by the time we collected the proteins, the effect had decreased and that is why we did not observe a full depletion of cMYC, p. cMYC or p. ERK, and consequently of FRA1 and p. FRA1. In turn, the effect of the BRAF inhibition was completely lost on the level of EZH2 and EED, which are farther downstream of BRAF compared to cMYC and FRA1. Interestingly, the effects of the anti-cancer drugs were not equal. Compared to vemurafenib, encorafenib exerted a stronger inhibitory effect, that is reflected by lower phosphorylation of ERK that in turn resulted in a lower expression and phosphorylation of FRA1 in T10 (Fig. 3). We also observed that H3K27me3 expression was higher only in vemurafenib-treated wells (Fig. 3). Although there is a high variation in H3K27me3, possibly due to the heterogenous expression of the histone H3 itself, we speculate that the initial BRAF blockade downregulated EZH2 and its target H3K27me3, and that is visible on the blots (Fig. 3). The differential effect of the chemotherapeuticals can be explained by their differing mechanism of action. Encorafenib is a general inhibitor of BRAF kinase activity regardless of being mutant or wild type [105]. However, vemurafenib specifically inhibits the kinase of *BRAF*-V600E mutant [104]. The *BRAF*-V600E mutants used in this study are heterozygous for the V600E mutation. That is possibly why encorafenib seems to have a stronger effect, as it abolishes BRAF activity entirely, whereas the vemurafenib only blocks the mutant kinase, and not the wild type, which remains functional. To improve this assay, we advise to resupply the chemotherapies daily, or to collect the samples earlier to ensure that the drugs are still active in the cells.

To test if FRA1 specifically interacts with the PRC2 core components in *BRAF*-V600E mutant organoids, we used small interfering RNA to block *FOSL1* transcription and therefore FRA1 protein translation. The inhibition of *FOSL1* was reflected on *mRNA* and on protein level in T10, which indicates that the treatment was successful (Fig. 4). However, there was a discrepancy between FRA1-inhibited *FOSL1* and FRA1 in NC (Fig. 4). Although *FOSL1* seems to be overexpressed following siFOSL1 treatment, the expression and phosphorylation of FRA1 on a protein level was low or completely diminished, further indicating that the transfection with siRNA was successful (Fig. 4). However, RT-PCR results from a single experiment are insufficient in reflecting a true biological effect due to the lack of biological repeats. The experiment has to be reproduced multiple times to narrow the error rate and to calculate the differences in variation in order to obtain a reliable outcome. Of note, we cannot make definitive conclusions about the effect of siFOSL1 on PRC2 genes, however, we recorded small decrease in all genes except for *EED*. These insignificant changes were not detected on a protein level for EZH2 and EED, suggesting that FRA1 has no involvement in the regulation of PRC2 core components. Histone H3 expression was homogenous in all lanes (Fig. 4), in contrast to the previous blot (Fig. 3), and therefore is a reliable loading control for the H3K27me3 mark. H3K27me3 showed increased expression in T10 compared to NC. Moreover, inhibition of FRA1 increased the H3K27me3 mark in T10, a difference that is not reflected by EZH2 expression (Fig. 4, B). We believe that such discrepancies could be a function of the assay itself as there is an increased possibility for technical errors in each component of the siRNA RT-PCR experiment. Small inhibitory RNA could yield very powerful gene transcription abrogation, in easily transfected cells such as Hela cells, however, transfection of higher order systems such as organoids could be challenging due to heterogeneous reagent dispersal and inappropriate siRNA delivery, among other problems [106,107]. In addition, the RT-PCR technique is known to be notoriously error-prone due to pipetting errors, evaporation, air entrapment, excluding other factors such as the quality of the template. Despite the limitations of the siRNA RT-PCR assay, on protein level, there is a visible decrease of FRA1 in siFOSL1-treated wells, indicating that the small inhibitory RNA treatment was successful, but no effect on EED, EZH2 and H3K27me3 was observed. CMYC, ERK and their phosphorylated versions were unaffected by FRA1 phosphorylation which makes sense because ERK is upstream of FRA1 and cMYC is not a target of FRA1 and therefore either should not be affected by blockade of FRA1. To further delve into FRA1 involvement with the PRC2 we performed ChIP and analysed it with RT-PCR. Due to poor primer design and a high degree of errors associated with the chromatin extraction and RT-PCR, we could not address this aim, and more biological repeats are required. However, the FRA1 enrichment is following a similar pattern in all lines and in all genes whereby FRA1 has the highest percentages in the BC2 line, followed by ~1% in the BC1 and NC lines, and no enrichment in the T10 line (Fig. 8, B). The observed pattern in all genes is suggesting that FRA1 occupation on PRC2 promoters is not dependent on BRAF status (Fig. 8, B), and that is also in line with the results following BRAF and *FOSL1* inhibition (Fig. 3, 7).

An important limitation of this experimental set-up is the presence of cMYC. *BRAF*-V600E-mediated overexpression of cMYC is known to regulate

H3K27me3 via direct interaction with the PRC2 genes [92]. Therefore, the presence of cMYC might prevent seeing any effect of FRA1 possibly due to competition for the same DNA binding site on EZH2 and other PRC2 components. To improve this setback, we advise the conditional knockdown of cMYC to exclude its already established regulatory role on the PRC2 complex, followed by transient deprivation from FRA1. Inducible constructs have an advantage over gene knockouts in that permanent inhibition especially of a key gene such as cMYC might have a detrimental effect on vital cellular processes. Resupplying the cells with FRA1 and/or cMYC would reveal specific effects on the PRC2 complex. Markers like gene and protein expression could be monitored as well as changes in methylation. Data from such analyses would enrich our understanding of FRA1 and cMYC in proliferation and stemness that has direct implications on metastatic cancer research.

Although our results did not support previous claims that FRA1 interacts with the PRC2 complex, FRA1 could be involved in epithelial cell transformations through a different mechanism. Due to strong evidence of FRA1 being involved in cell motility, we used a metastasis-promoting matrix to compare differences in morphology between FRA1-high BRAF-V600E mutant CRC organoids with *BRAF*-wt that have low levels of FRA1. We discovered that lines carrying the *BRAF*-V600E mutation promoted cell protrusions and separating cells in Collagen I and not in BME, whereas *BRAF*-corrected lines did not form cell sprouts in either matrix (Fig. 5; Fig. 6, B; Fig. 7, A). Similar to Koorman et al, we observed small protrusions when the collagen was polymerised at 37ºC, however, a collective invasion of bigger sprouts occurred at 26ºC, likely due to larger pore formation and a higher alignment of the collagen [91]. Upon use of BRAF inhibitors we partially abolished sprout formation, indicating that BRAF is upstream of molecular events responsible for the aberrant phenotype (Fig. 7). The sprouting events are reminiscent of pseudo-like cytoplasmic protrusions that have been described in EMT-derived tumour cells clustering predominantly on the invasive front of the tumour. Moreover, we observed detached cells or cell debris that might follow a similar mechanism to tumour budding, however, further research is required (Fig. 6, A). Similar to what we observed, these protrusions are often in direct contact with adjacent structures and along with the budding cells are associated with increased cell motility and invasiveness [108–111]. Tumour budding is associated with certain parameters notably loss of clear sprouting or cell budding, however, more scientific effort is required to unravel the relationship between FRA1 and the Rho-pathway.

boundary between tumour and healthy tissue, and cell migration, and has been officially recognised as additional prognostic factor by the international union against cancer (UICC) [112–114]. Utilising the Collagen I assay to model invasion and possibly a process similar to tumour budding could be developed into a useful prognostic marker for patients in the future.

From our experiments we can only speculate if the detached cells are indeed living and migrating away from the organoids. That is why including a cell tracking assay or using a live/dead stain would provide clarification. Following this, to understand the role of FRA1 in BRAF-V600E overexpression, it would be useful to generate FRA1 mutant for its essential phosphorylation sites. That way FRA1 would be specifically prevented from *BRAF*-ERK-mediated activation, and thereby would confirm that any effects produced by FRA1 are due to the *BRAF*-V600E mutation. From that, RNA sequencing and protein expression would give insight into FRA1-mediated molecular shifts. Furthermore, changes in morphology can be assessed with the 3D sprouting assay in Collagen I. Chemoattractants characteristic of metastatic CRC can also be included to test the migration ability of organoid budding cells. Overall, the 3D sprouting in Collagen I can be used to monitor organoid morphology and is a powerful tool to test novel cancer drugs that provides a possibility for personalised patient approach.

Despite the correlations between FRA1 expression and EZH2 activity in EMT, according to our research, FRA1 does not affect PRC2 expression on *mRNA* or protein level. Rather than via the PRC2 complex, FRA1 could contribute to invasive behaviour in another way. There is extensive literature on FRA1's involvement in cell motility through cytoskeletal rearrangements. For example, it has been clearly demonstrated that the MAPK/ERK-induced overexpression of FRA1 leads to inhibition of ROCK signalling which is necessary for the extension of ruffles into active extending protrusions in colon carcinoma cells [100]. Moreover, inhibition of FRA1 decreased tumour cell motility and invasion. Of note, in our 3D sprouting experiment with the mutant T10 in Collagen I vs BME, we observed no added value of including ROCK inhibitor on protrusion formation or cell migration (Fig. 6). Vial et al demonstrated that overactivated FRA1 plays the same function as pharmacologically inhibiting the ROCK pathway, that serves to prevent cells dying from anoikis [95,100]. For that reason, we speculate that, upon addition of the drug there was no increase in

Conclusions

Our goal was to decipher potential mechanisms of *BRAF*-V600E-induced FRA1 in metastatic CRC. We confirmed that FRA1 is overexpressed due to *BRAF*-V600E overactive kinase activity and that *BRAF*-V600E is specifically responsible for acquiring an invasive phenotype in CRC. Therefore, we hypothesised that FRA1 is involved in promoting invasion possibly through the PRC2 complex, however, we could not identify relevant molecular interactions with FRA1. It is possible that FRA1 contributes to cancer aggressiveness via a different route, through cytoskeletal rearrangements and evading anoikis, through interaction with ROCK signalling, for instance. Albeit lacking the complexity of a whole organism, patient-derived organoids are comparable to the tissue of origin and carry patient-specific features. Our model system of CRC and invasion can be used to test novel chemotherapy drugs in combination with genome-editing technology to specifically target FRA1, in order to fully unravel its roles in CRC. The 3D nature of the organoid system allows the spatiotemporal investigation of protein localisation and cytoskeletal elements utilising techniques like immunohistochemistry and live imaging. These techniques can be combined to improve our experimental set-up to build up our knowledge of FRA1 in the setting of *BRAF*-V600E.

Acknowledgements

We thank Daan Visser from the Derksen group for helping to fine-tune the 3D sprouting assays in Collagen I and gifting us the Collagen I GFP probe, and Madelon Maurice from the Stratenum part of the University Medical Centre Utrecht for supplying us with materials. On a personal note, I would like to thank all members of the LTO, specifically Professor Dr. Onno Kranenburg for inviting me for this project, and deepest gratitude to Layla El Bouazzaoui for the constructive feedback and emotional support throughout my project.

Bibliography

1. Holmes, D. A disease of growth. *Nature 2015 521:7551* **521**, S2–S3 (2015).
2. Colorectal Cancer Statistics | CDC. https://www.cdc.gov/cancer/colorectal/statistics/index.htm.
3. Bray, F. *et al.* Global cancer statistics 2018: GLOBOCAN estimates of incidence and mortality worldwide for 36 cancers in 185 countries. *CA Cancer J Clin* **68**, 394–424 (2018).
4. Sung, H. *et al.* Global Cancer Statistics 2020: GLOBOCAN Estimates of Incidence and Mortality Worldwide for 36 Cancers in 185 Countries. *CA Cancer J Clin* **71**, 209–249 (2021).
5. Arnold, M. *et al.* Global patterns and trends in colorectal cancer incidence and mortality. *Gut* **66**, 683–691 (2017).
6. Hofseth, L. J. *et al.* Early-onset colorectal cancer: initial clues and current views. *Nat Rev Gastroenterol Hepatol* **17**, 352–364 (2020).
7. Dekker, E. *et al.* Colorectal cancer. *The Lancet* **394**, 1467–1480 (2019).
8. Munro, M. *et al*. Cancer stem cells in colorectal cancer: a review. *J Clin Pathol* **71**, 110–116 (2018).
9. Simon, K. Colorectal cancer development and advances in screening. *Clin Interv Aging* **11**, 967 (2016).
10. Colorectal Cancer — Cancer Stat Facts. https://seer.cancer.gov/statfacts/html/colorect.html.
11. Muzny, D. M. *et al.* Comprehensive molecular characterization of human colon and rectal cancer. *Nature 2012 487:7407* **487**, 330–337 (2012).
12. Fearon, E. R. & Vogelstein, B. A genetic model for colorectal tumorigenesis. *Cell* **61**, 759–767 (1990).
13. Estellar, M. Analysis of Adenomatous Polyposis Coli Promoter Hypermethylation in Human Cancer. *Cancer Research* 60(16): 4366-4371 https://aacrjournals-org.proxy.library.uu.nl/cancerres/article/60/16/4366/506589/Analysis-of-Adenomatous-Polyposis-Coli-Promoter (2000).
14. Powell, S. M. *et al.* APC mutations occur early during colorectal tumorigenesis. *Nature* **359**, 235–237 (1992).
15. Pino, M. S. & Chung, D. C. THE CHROMOSOMAL INSTABILITY PATHWAY IN COLON CANCER. *Gastroenterology* **138**, 2059 (2010).
16. Clevers, H. Wnt/beta-catenin signaling in development and disease. *Cell* **127**, 469–480 (2006).
17. Barker, N. *et al.* Crypt stem cells as the cells-of-origin of intestinal cancer. *Nature* **457**, 608–611 (2009).

18. Parker, T. W. & Neufeld, K. L. APC controls Wnt-induced β-catenin destruction complex recruitment in human colonocytes. *Sci Rep* **10**, (2020).
19. Stanczak, A. *et al.* Prognostic significance of Wnt-1, β-catenin and E-cadherin expression in advanced colorectal carcinoma. *Pathol Oncol Res* **17**, 955–963 (2011).
20. Mann, B. *et al.* Target genes of β-catenin–T cell-factor/lymphoid-enhancer-factor signaling in human colorectal carcinomas. *Proc Natl Acad Sci U S A* **96**, 1603 (1999).
21. Watanabe, K. *et al.* Integrative ChIP-seq/Microarray Analysis Identifies a CTNNB1 Target Signature Enriched in Intestinal Stem Cells and Colon Cancer. *PLoS One* **9**, (2014).
22. Dhillon, A. *et al.* MAP kinase signalling pathways in cancer. *Oncogene 2007 26:22* **26**, 3279–3290 (2007).
23. Pylayeva-Gupta, Y. *et al.* RAS oncogenes: weaving a tumorigenic web. *Nat Rev Cancer* **11**, 761–774 (2011).
24. Degirmenci, U. *et al.* Targeting Aberrant RAS/RAF/MEK/ERK Signaling for Cancer Therapy. *Cells* **9**, (2020).
25. Haigis, K. M. *et al.* Differential effects of oncogenic K-Ras and N-Ras on proliferation, differentiation and tumor progression in the colon. *Nat Genet* **40**, 600 (2008).
26. Santini, D. *et al.* High concordance of KRAS status between primary colorectal tumors and related metastatic sites: implications for clinical practice. *Oncologist* **13**, 1270–1275 (2008).
27. Baker, S. J. *et al.* Chromosome 17 deletions and p53 gene mutations in colorectal carcinomas. *Science* **244**, 217–221 (1989).
28. Jass, J. R. & Smirth, M. Sialic acid and epithelial differentiation in colorectal polyps and cancer--a morphological, mucin and lectin histochemical study. *Pathology* **24**, 233–242 (1992).
29. Kim, S. Y. & Kim, T. il. Serrated neoplasia pathway as an alternative route of colorectal cancer carcinogenesis. *Intest Res* **16**, 358 (2018).
30. Antonios Margonis, G. *et al.* Association of BRAF Mutations With Survival and Recurrence in Surgically Treated Patients With Metastatic Colorectal Liver Cancer Supplemental content. *JAMA Surg* **153**, 180996 (2018).
31. Bond, C. E. & Whitehall, V. L. J. How the BRAF V600E mutation defines a distinct subgroup of colorectal cancer: Molecular and clinical implications. *Gastroenterol Res Pract* **2018**, (2018).
32. Samowitz, W. S. *et al.* Poor Survival Associated with the BRAF V600E Mutation in Microsatellite-Stable Colon Cancers. *Cancer Res* **65**, 6063–6069 (2005).
33. Jen, J. *Molecular determinants of dysplasia in colorectal lesions*. http://aacrjournals.org/cancerres/article-pdf/54/21/5523/2455342/cr0540215523.pdf (1994).
34. Dehari, R. Infrequent APC mutations in serrated adenoma. *Tohoku J Exp Med* **193**, 181–186 (2001).
35. Sawyer, E. J. *et al.* Molecular characteristics of serrated adenomas of the colorectum. *Gut* **51**, 200–206 (2002).
36. Rosenberg, D. W. *et al.* Mutations in BRAF and KRAS differentially distinguish serrated versus non-serrated hyperplastic aberrant crypt foci in humans. *Cancer Res* **67**, 3551–3554 (2007).
37. Brummer, T. & Röring, M. Aberrant B-Raf signaling in human cancer -- 10 years from bench to bedside. *Crit Rev Oncog* **17**, 97–121 (2012).
38. Rajagopalan, H. *et al.* Tumorigenesis: RAF/RAS oncogenes and mismatch-repair status. *Nature* **418**, 934 (2002).
39. Stefanius, K. *et al.* Frequent mutations of KRAS in addition to BRAF in colorectal serrated adenocarcinoma. *Histopathology* **58**, 679–692 (2011).
40. Bettington, M. *et al.* The serrated pathway to colorectal carcinoma: current concepts and challenges. *Histopathology* **62**, 367–386 (2013).
41. Morkel, M. *et al.* Similar but different: distinct roles for KRAS and BRAF oncogenes in colorectal cancer development and therapy resistance. *Oncotarget* **6**, 20785 (2015).
42. Yan, H. H. N. *et al.* RNF43 germline and somatic mutation in serrated neoplasia pathway and its association with BRAF mutation. *Gut* **66**, 1645–1656 (2017).
43. Matsumoto, A. *et al.* RNF43 mutation is associated with aggressive tumor biology

along with BRAF V600E mutation in right-sided colorectal cancer. *Oncol Rep* **43**, 1853–1862 (2020).
44. Dienstmann, R. *et al.* Consensus molecular subtypes and the evolution of precision medicine in colorectal cancer. *Nat Rev Cancer* **17**, 79–92 (2017).
45. Bugter, J. *et al.* Mutations and mechanisms of WNT pathway tumour suppressors in cancer. *Nature Reviews Cancer 2020 21:1* **21**, 5–21 (2020).
46. Radaszkiewicz, T. *et al.* RNF43 inhibits WNT5A-driven signaling and suppresses melanoma invasion and resistance to the targeted therapy. *Elife* **10**, (2021).
47. Wan, P. T. C. *et al.* Mechanism of activation of the RAF-ERK signaling pathway by oncogenic mutations of B-RAF. *Cell* **116**, 855–867 (2004).
48. Davies, H. *et al.* Mutations of the BRAF gene in human cancer. *Nature 2002 417:6892* **417**, 949–954 (2002).
49. Yao, Z. *et al.* BRAF mutants evade ERK dependent feedback by different mechanisms that determine their sensitivity to pharmacologic inhibition. *Cancer Cell* **28**, 370 (2015).
50. Angel, P. & Karin, M. The role of Jun, Fos and the AP-1 complex in cell-proliferation and transformation. 129–157 (1991).
51. Shaulian, E. & Karin, M. AP-1 in cell proliferation and survival. *Oncogene 2001 20:19* **20**, 2390–2400 (2001).
52. Lee, W. *et al.* Purified transcription factor AP-1 interacts with TPA-inducible enhancer elements. *Cell* **49**, 741–752 (1987).
53. Angel, P. *et al.* Phorbol ester-inducible genes contain a common cis element recognized by a TPA-modulated trans-acting factor. *Cell* **49**, 729–739 (1987).
54. Eckert, R. L. *et al.* AP1 Transcription Factors in Epidermal Differentiation and Skin Cancer. *J Skin Cancer* **2013**, 1–9 (2013).
55. Karin, M. The Regulation of AP-1 Activity by Mitogen-activated Protein Kinases *. *Journal of Biological Chemistry* **270**, 16483–16486 (1995).
56. Mechta, F. *et al.* Transformation by ras modifies AP1 composition and activity. *Oncogene* **14**, 837–847 (1997).
57. Raivich, G. & Behrens, A. Role of the AP-1 transcription factor c-Jun in developing, adult and injured brain. *Prog Neurobiol* **78**, 347–363 (2006).
58. Terasawa, K. *et al.* Regulation of c-Fos and Fra-1 by the MEK5-ERK5 pathway. *Genes to Cells* **8**, 263–273 (2003).
59. Tower, G. *et al.* Fra-1 targets the AP-1 site/2G single nucleotide polymorphism (ETS site) in the MMP-1 promoter. *Eur J Biochem* **270**, 4216–4225 (2003).
60. Gruda, M. *et al.* Regulation of Fra-1 and Fra-2 phosphorylation differs during the cell cycle of fibroblasts and phosphorylation in vitro by MAP kinase affects DNA binding activity. *undefined* (1994).
61. Doehn, U. *et al.* RSK Is a Principal Effector of the RAS-ERK Pathway for Eliciting a Coordinate Promotile/Invasive Gene Program and Phenotype in Epithelial Cells. *Mol Cell* **35**, 511–522 (2009).
62. Treinies, I. *et al. Activated MEK Stimulates Expression of AP-1 Components Independently of Phosphatidylinositol 3-Kinase (PI3-Kinase) but Requires a PI3-Kinase Signal To Stimulate DNA Synthesis*. *MOLECULAR AND CELLULAR BIOLOGY* vol. 19 https://journals.asm.org/journal/mcb (1999).
63. Song, Y. *et al.* An association of a simultaneous nuclear and cytoplasmic localization of Fra-1 with breast malignancy. *BMC Cancer 2006 6:1* **6**, 1–7 (2006).
64. Logullo, A. F. *et al.* Role of Fos-related antigen 1 in the progression and prognosis of ductal breast carcinoma. *Histopathology* **58**, 617–625 (2011).
65. Nakajima, H. *et al.* Aberrant Expression of Fra-1 in Estrogen Receptor-negative Breast Cancers and Suppression of their Propagation In Vivo by Ascochlorin, an Antibiotic that Inhibits Cellular Activator Protein-1 Activity. *The Journal of Antibiotics 2007 60:11* **60**, 682–689 (2007).
66. Wykosky, J. *et al.* Interleukin-13 Receptor α2, EphA2, and Fos-Related Antigen 1 as Molecular Denominators of High-Grade Astrocytomas and Specific Targets for Combinatorial Therapy. *Clinical Cancer Research* **14**, 199–208 (2008).
67. Kim, Y.-H. *et al.* Fra-1 Expression in Malignant and Benign Thyroid Tumor. *Korean J Intern Med* **16**, 93–97 (2001).

68. Marques, C. *et al.* Nf1 regulates mesenchymal glioblastoma plasticity and aggressiveness through the ap-1 transcription factor fosl1. *Elife* **10**, (2021).
69. Dong, J. *et al.* Transcriptional super-enhancers control cancer stemness and metastasis genes in squamous cell carcinoma. *Nature Communications 2021 12:1* **12**, 1–14 (2021).
70. Diesch, J. *et al.* Widespread FRA1-Dependent Control of Mesenchymal Transdifferentiation Programs in Colorectal Cancer Cells. *PLoS One* **9**, e88950 (2014).
71. Liu, H. *et al.* Aberrantly expressed Fra-1 by IL-6/STAT3 transactivation promotes colorectal cancer aggressiveness through epithelial–mesenchymal transition. *Carcinogenesis* **36**, 459 (2015).
72. Zhang, W. *et al.* Differential Expression of the AP-1 Transcription Factor Family Members in Human Colorectal Epithelial and Neuroendocrine Neoplasms. *Am J Clin Pathol* **124**, 11–19 (2005).
73. L, Z. *et al.* Fos-related activator-1 is overexpressed in oral squamous cell carcinoma and associated with tumor lymph node metastasis. *J Oral Pathol Med* **39**, 470–476 (2010).
74. Iskit, S. *et al.* Fra-1 is a key driver of colon cancer metastasis and a Fra-1 classifier predicts disease-free survival. *Oncotarget* **6**, 43146 (2015).
75. Vial, E. *et al. ERK-MAPK signaling coordinately regulates activity of Rac1 and RhoA for tumor cell motility*. http://www.cancercell.org/cgi/content/full/4/1/67/DC1 (2003).
76. Stelniec-Klotz, I. *et al.* Reverse engineering a hierarchical regulatory network downstream of oncogenic KRAS. *Mol Syst Biol* **8**, 601 (2012).
77. Bakiri, L. *et al.* Fra-1/AP-1 induces EMT in mammary epithelial cells by modulating Zeb1/2 and TGFβ expression. *Cell Death & Differentiation 2015 22:2* **22**, 336–350 (2014).
78. Zhao, C. *et al.* Genome-wide Profiling of AP-1–Regulated Transcription Provides Insights into the Invasiveness of Triple-Negative Breast Cancer. *Cancer Res* **74**, 3983–3994 (2014).
79. Thiery, J. P. *et al.* Epithelial-mesenchymal transitions in development and disease. *Cell* **139**, 871–890 (2009).
80. Zlobec, I. *et al.* Epithelial mesenchymal transition and tumor budding in aggressive colorectal cancer: Tumor budding as oncotarget. *Oncotarget* **1**, 651–661 (2010).
81. Yu, M. *et al.* Circulating Breast Tumor Cells Exhibit Dynamic Changes in Epithelial and Mesenchymal Composition. *Science (1979)* **339**, 580–584 (2013).
82. Brabletz, T. To differentiate or not — routes towards metastasis. *Nature Reviews Cancer 2012 12:6* **12**, 425–436 (2012).
83. Evellin, S. *et al.* FOSL1 Controls the Assembly of Endothelial Cells into Capillary Tubes by Direct Repression of αv and β3 Integrin Transcription. *Mol Cell Biol* **33**, 1198–1209 (2013).
84. Ferraro, A. *et al.* EZH2 is regulated by ERK/AKT and targets integrin alpha2 gene to control Epithelial–Mesenchymal Transition and anoikis in colon cancer cells. *Int J Biochem Cell Biol* **45**, 243–254 (2013).
85. O'Meara, M. M. & Simon, J. A. Inner workings and regulatory inputs that control Polycomb repressive complex 2. *Chromosoma* **121**, 221 (2012).
86. Margueron, R. & Reinberg, D. The Polycomb complex PRC2 and its mark in life. *Nature 2011 469:7330* **469**, 343–349 (2011).
87. Sobolev, V. v. *et al.* Role of the Transcription Factor FOSL1 in Organ Development and Tumorigenesis. *Int J Mol Sci* **23**, (2022).
88. Jiang, X. *et al.* Expression and function of FRA1 protein in tumors. *Molecular Biology Reports 2019 47:1* **47**, 737–752 (2019).
89. Brauchle, E. *et al.* Biomechanical and biomolecular characterization of extracellular matrix structures in human colon carcinomas. *Matrix Biology* **68–69**, 180–193 (2018).
90. Karlsson, S. & Nyström, H. The extracellular matrix in colorectal cancer and its metastatic settling – Alterations and biological implications. *Crit Rev Oncol Hematol* **175**, 103712 (2022).
91. Koorman, T. *et al.* Spatial collagen stiffening promotes collective breast cancer cell invasion by reinforcing extracellular matrix alignment. *Oncogene* **41**, 2458–2469 (2022).
92. Qu, Y. *et al.* C-Myc is required for BRAFV600E-induced epigenetic silencing

by H3K27me3 in tumorigenesis. *Theranostics* **7**, 2092–2107 (2017).
93. Sullivan, A. E. & Santos, S. D. M. An Optimized Protocol for ChIP-Seq from Human Embryonic Stem Cell Cultures. *STAR Protoc* **1**, (2020).
94. Hake, S. B. *et al.* Expression patterns and post-translational modifications associated with mammalian histone H3 variants. *J Biol Chem* **281**, 559–568 (2006).
95. Wang, X. *et al.* Inhibition of Caspase-mediated Anoikis Is Critical for Basic Fibroblast Growth Factor-sustained Culture of Human Pluripotent Stem Cells. *J Biol Chem* **284**, 34054 (2009).
96. McGrath, P. S. & Wells, J. M. SnapShot: GI tract development. *Cell* **161**, 176.e1-176.e1 (2015).
97. Lea, T. Caco-2 Cell Line. 103–111 (2015) doi:10.1007/978-3-319-16104-4_10.
98. Sato, T. *et al.* Single Lgr5 stem cells build crypt-villus structures in vitro without a mesenchymal niche. *Nature* **459**, 262–265 (2009).
99. Bustin, S. A. *et al.* The MIQE Guidelines: Minimum Information for Publication of Quantitative Real-Time PCR Experiments. *Clin Chem* **55**, 611–622 (2009).
100. Vial, E. *et al.* MAPK signaling coordinately regulates activity of Rac1 and RhoA for tumor cell motility. *Cancer Cell* **4**, 67–79 (2003).
101. Rock, W. D. *et al.* Effects of KRAS, BRAF, NRAS, and PIK3CA mutations on the efficacy of cetuximab plus chemotherapy in chemotherapy-refractory metastatic colorectal cancer: a retrospective consortium analysis. *Lancet Oncol* **11**, 753–762 (2010).
102. Barras, D. *et al.* BRAF V600E Mutant Colorectal Cancer Subtypes Based on Gene Expression. *Clin Cancer Res* **23**, 104–115 (2017).
103. Liu, H. *et al.* Aberrantly expressed Fra-1 by IL-6/STAT3 transactivation promotes colorectal cancer aggressiveness through epithelial-mesenchymal transition. *Carcinogenesis* **36**, 459–468 (2015).
104. Zhang, W. *et al.* Clinical Pharmacokinetics of Vemurafenib. *Clinical Pharmacokinetics 2017 56:9* **56**, 1033–1043 (2017).
105. CHMP. Committee for Medicinal Products for Human Use (CHMP) Assessment report. (2018).
106. Bhise, N. S. *et al.* The relationship between terminal functionalization and molecular weight of a gene delivery polymer and transfection efficacy in mammary epithelial 2-D cultures and 3-D organotypic cultures. *Biomaterials* **31**, 8088–8096 (2010).
107. McManus, M. T. & Sharp, P. A. Gene silencing in mammals by small interfering RNAs. *Nature Reviews Genetics 2002 3:10* **3**, 737–747 (2002).
108. Shinto, E. *et al.* A novel classification of tumour budding in colorectal cancer based on the presence of cytoplasmic pseudo-fragments around budding foci. *Histopathology* **47**, 25–31 (2005).
109. Guarino, M. *et al.* The role of epithelial-mesenchymal transition in cancer pathology. *Pathology* **39**, 305–318 (2007).
110. Ueno, H. *et al.* Tumour 'budding' as an index to estimate the potential of aggressiveness in rectal cancer. *Histopathology* **40**, 127–132 (2002).
111. Koelzer, V. *et al.* Tumor budding in colorectal cancer—ready for diagnostic practice? *Hum Pathol* **47**, 4–19 (2016).
112. Compton, C.C. *et al.* Prognostic factors in colorectal cancer. College of American Pathologists Consensus Statement 1999. *Arch Pathol Lab Med* **124**, 43–53 (2000).
113. Brabletz, T. *et al.* Opinion: migrating cancer stem cells - an integrated concept of malignant tumour progression. *Nat Rev Cancer* **5**, 744–749 (2005).
114. H, U. *et al.* Predictors of extrahepatic recurrence after resection of colorectal liver metastases. *Br J Surg* **91**, 327–333 (2004).

Supplementary materials

Reagents & antibodies	Catalogue number	Manufacturer
Advanced DMEM/F-12	12634010	ThermoFisher Scientific
A83-01	HY-10432	MCE
Basement membrane extract (BME)	3533-001-02	Sigma-Aldrich
Albumin Bovine Fraction V, powder	24040100	ThermoFisher Scientific
Bovine Serum Albumin Standard	5000206	Bio-Rad
B-27	17504044	ThermoFisher Scientific
c-myc (E5Q6W) Rabbit mAb	18583	Cell Signalling Technology
Cultrex Rat Collagen I	344000501	R&D
Cytokeratin 20 (M7019)	M7019	Agilent Dako
DAPI	422801	BioLegend
Dispase II, powder	17105041	ThermoFisher Scientific
ECL Prime Western Blotting Detection Reagent	10308449	Cytiva
EED (E4L6E) XP Rabbit mAb	85322	Cell Signalling Technology
EGF (human)		PreproTech
Encorafenib (LGX818)	S7108	Selleckchem
Ezh2 (D2C9) XP Rabbit mAb	5246	Cell Signalling Technology
FRA1 (D80B4) Rabbit mAb	5281	Cell Signalling Technology
GAPDH (D16H11) XP Rabbit mAb	cs5174	Cell Signalling Technology
Glutamax Supplement		ThermoFisher Scientific
Goat-anti-mouse IgG (H+L) Secondary Ab Alexa Fluor 688	A21057	Life technology
Goat-anti-mouse Polyclonal immunoglobulins HRP	P0448	Agilent Dako
Goat-anti-rabbit Polyclonal immunoglobuling HRP	P0447	Agilent Dako
GoTaq DNA Polymerase	M3005	Promega
HEPES	H3375	Sigma
High Pure PCR Product Pufirication Kit	11732676001	Roche
H3 Rabbit pAb	ab1791	Abcam
H3K27me3 (C36B11) Rabbit mAb	cst9733	Cell Signalling Technology
INTERFERin, siRNA and miRNA Transfection Reagent	101000036	Polyplus
iScript Reverse Transcription Supermix	1708891	Bio-Rad
IQ SYBR Green Supermix	1708882	Bio-Rad
MAPK Erk1/2 p44/42 (137F5) Rabbit mAb	cst4695	Cell Signalling Technology
MAPK p. Erk1/2 p44/42 Thr202/Tyr204 Rabbit Ab	9101	Cell Signalling Technology
µ-slide (immunofluorescence)	81506	Ibidi
Mounting medium	50001	Ibidi
N-acetyl-L-cysteine	A9165	Sigma
Nicotinamide	N0636	Sigma
ON-TARGET plus Non-targeting Control Pool	D0018101005	PerkinElmer (horizon)
Opti-MEM Reduced Serum Media		ThermoFisher Scientific
PageRuler Plus Prestained Protein Ladder (10 to 250 kDa)	26619	ThermoFisher Scientific
p. c-Myc Ser62 (E1J4K) Rabbit mAb	13748	Cell signalling
Penicilin/Streptomycin (P/S)		ThermoFisher Scientific
pET28a-EGFP-CNA35 (Collagen I probe)	61603	Addgene
p. FRA1 Ser265 (D22B1) Rabbit mAb	5841	Cell Signalling Technology
Protein Assay Dye Reagent Concentrate	5000006	Bio-Rad
QIAamp DNA Micro Kit	56304	QIAGEN
RIPA (lysis buffer)	9806	Cell Signalling Technology
RNeasy Micro Kit	74004	QIAGEN
SB202190	A1632	Gentaur
siRNA Human FOSL1 ON-TARGET plus SMART pool	L004341000005	PerkinElmer (Dharmacon Reagents)
Trans-Blot Turbo Transfer system	1704150	Bio-Rad
Trans-Blot Turbo Midi Nitrocellulose Transfer Packs	1704159	Bio-Rad
TrypLE		ThermoFisher Scientific
Vemurafenib	PLX4032	Selleckhem
Y-27632 (ROCK inhibitor)	HY-10583	MedChem Express

Supplementary Table 1. Reagents and antibodies catalogue sheet.

ChIP RT-PCR

Target	Sequence	Transcription factor
1. EZH2 Promoter I	FW: TCCACTGCCTTCTGAGTCC RV: AAAGCGATGGCGATTGGG	FRA1/cMYC
2. EZH2 Promoter II	FW: CTCCACTGCCTTCTGAGTCC RV: CCCTGTGATTGGACGGGC	FRA1/cMYC
3. EED Promoter	FW: TTCCACAGACTTTCGCTCCC RV: CCGGCAGTCTACACGATGTA	FRA1/cMYC
4. SUZ12 Promoter	FW: GACCCCTAATTTTCCCGCGA RV: GGATTCCCCCGTCAGTCAC	FRA1
5. SUZ12 Promoter	FW: GATGGCGCCTCAGAAGCA RV: GATTTGCCGCCCGAAGCC	cMYC
6. Negative Control	FW: AGTCTCATTCGGTTGCCCAG RV: AGACCAGACTGGCCAACATG	hg19_dna range=chr12:49585004-49585919

siRNA RT-PCR

7. FRA1	FW: GGAGGAAGGAACTGACCGACTT RV: CCAGATTTCTCATCTTCCAGTTTGT
8. EZH2	FW: ATTTCGTAGGAGGGAGCAAAG RV: TGGGCCTGCTACTGTTATTG
9. EED	FW: TAAGGGCACGTAGAGCATTTAG RV: TGAGCAGGAAGACAGTACAAAG
10. SUZ12	FW: GCAGCTTACGTTTACTGGTTTC RV: TGAGTTTGGTGATGGCTTATCT
11. GAPDH	FW: CTTTTGCGTCGCCAG RV: TTGATGGCAACAATATCCAC

Genotyping

12. BRAF-V600E	FW: CAGACCTCTGACCTTGCTCA RV: GACAACTGTTCAAACTGATGGGA

Supplementary Table 2. Primer sets.

Primers are displayed in a 5’ to 3’ direction.

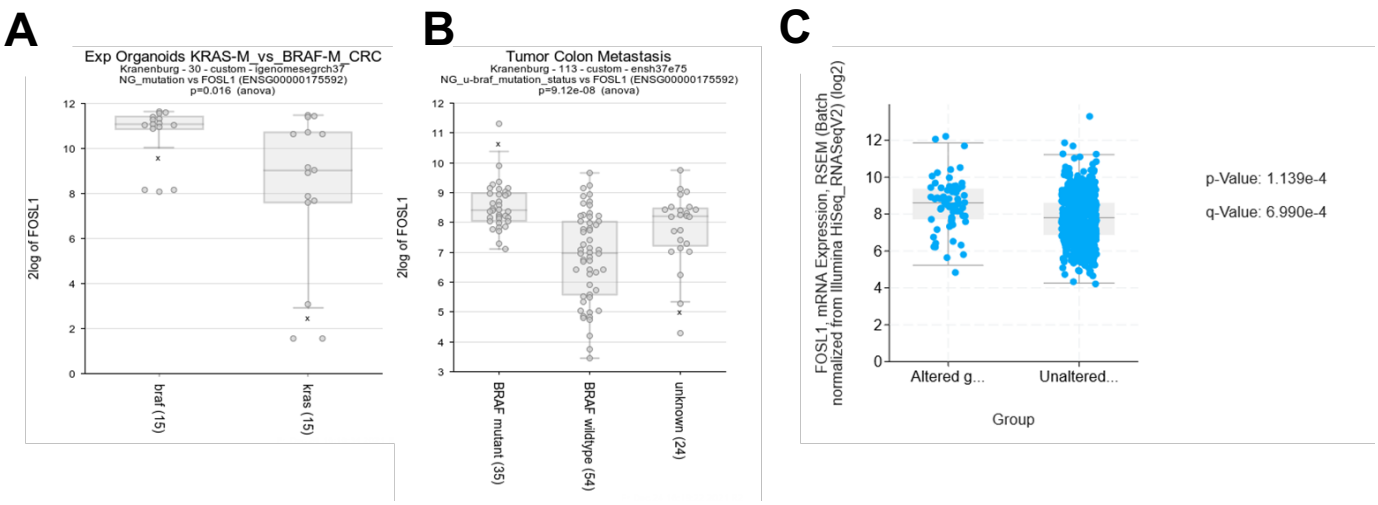

Supplementary figure 1. *FOSL1 mRNA* expression in colorectal cancer.

Data in A and B was obtained via *mRNA* sequencing by the Kranenburg group and graphs were generated in R2 Software (Amsterdam Medical Centre). The results published in C are based on the TCGA dataset generated in the cBioPortal.

(A) Expression of *FOSL1 mRNA* between 15 *KRAS* and 15 *BRAF* mutant in CRC organoids
(B) Expression of *FOSL1 mRNA* between 35 *BRAF* mutant, 54 *BRAF* wildtype and 24 unknown for the mutations in patient biopsies of tumour colon metastasis.
(C) Expression of *FOSL1 mRNA* between mutant *BRAF* (alterred) and wildtype *BRAF* (unaltered) in the TCGA cohort.

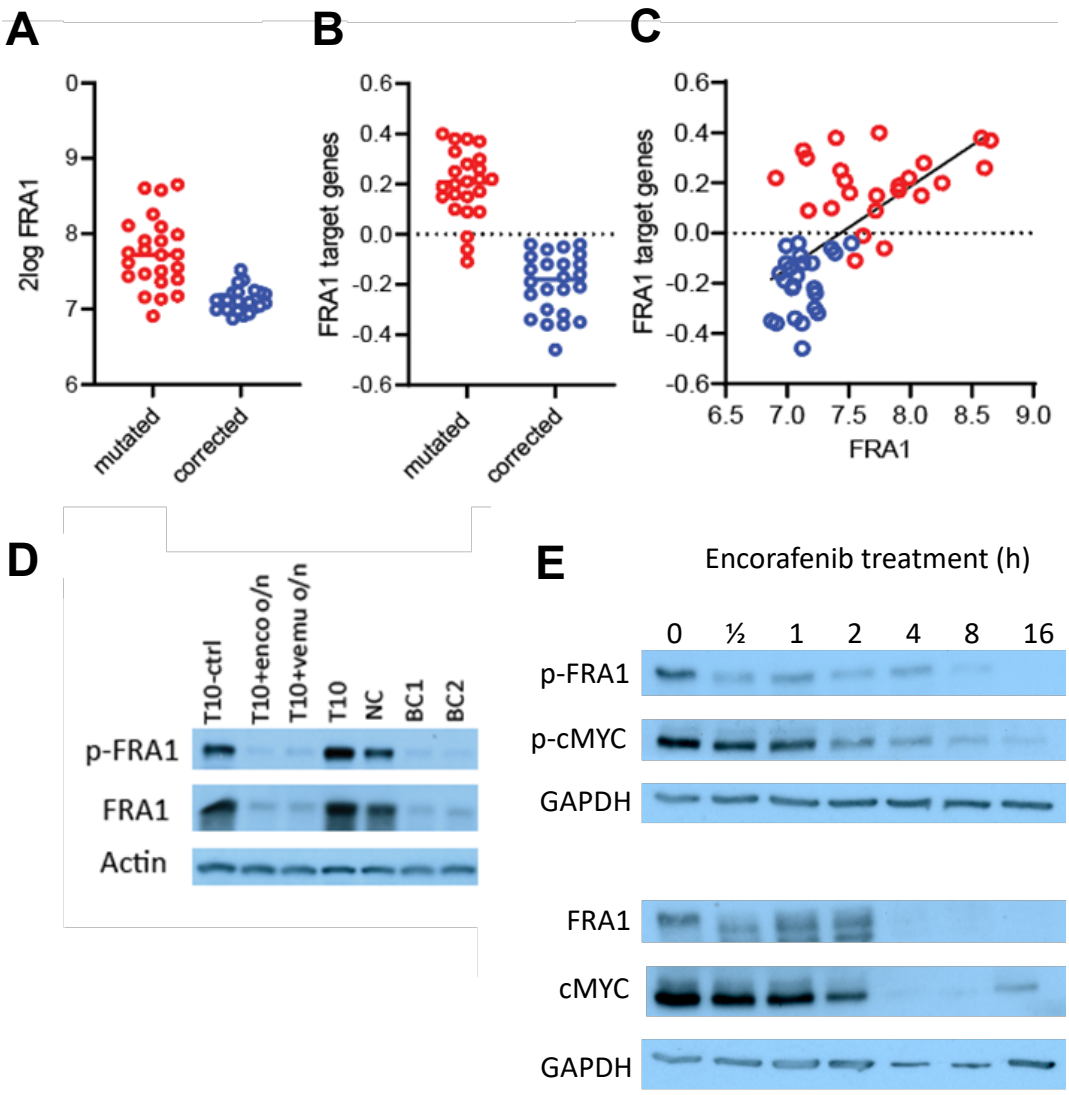

Supplementary figure 2. *FOSL1 mRNA* and FRA1 protein expression comparison between *BRAF*-V600E mutant and *BRAF*-corrected colorectal cancer organoids.

Data was generated via RNA sequencing by the Kranenburg group and the plots were made in R2 (Software by Amsterdam Medical Centre).

(A) *MRNA* expression of *FOSL1* in *BRAF*-V600E mutant (mutated) and *BRAF*-corrected (corrected) CRC organoids.
(B) *MRNA* expression of *FOSL1* target genes in *BRAF*-V600E mutant and *BRAF*-corrected CRC organoids.
(C) Correlation graph of A and B.
(D) Protein expression of phosphorylated FRA1 (p-FRA1) and FRA1 in *BRAF*-V600E (T10, NC) and *BRAF*-corrected (BC1, BC2). T10 was treated with encorafenib (enco o/n) or vemurafenib (vemu o/n) overnight. Actin was used as loading control.
(E) Following encorafenib treatment, protein expression of p-FRA1, FRA1, cMYC and phosphorylated cMYC (p-cMYC) was detected at different time points shown on the top of the blots. GAPDH was used as a loading control.